Salt marsh erosion rates and boundary features in a shallow Bay

Nicoletta Leonardi[1,2], Zafer Defne[3], Neil K. Ganju[3], Sergio Fagherazzi[2]

[1]Department of Geography and Planning, University of Liverpool, Liverpool, UK

[2]Department of Earth and Environment, Boston University, Boston , MA, USA

[3]United States Geological Survey, Woods Hole MA, USA

ABSTRACT

Herein, we investigate the relationship between wind waves, salt marsh erosion rates, and the planar shape of marsh boundaries by using aerial images and the numerical model COAWST. Using Barnegat Bay, New Jersey, as a test site, we found that salt marsh erosion rates maintain a similar trend in time. We also found a significant relationship between salt marsh erosion rates and the shape of marsh boundaries which could be used as a geomorphic indicator of the degradation level of the marsh. Slowly eroding salt marshes are irregularly shaped with fractal dimension higher than rapidly deteriorating marshes. Moreover, for low wave-energy conditions, there is a high probability of isolated and significantly larger than average failures of marsh portions causing a long-tailed distribution of localized erosion rates. Finally, we confirm the existence of a significant relationship between salt marsh erosion rate and wind waves exposure. Results suggest that variations in time in the morphology of salt marsh boundaries could be used to infer changes in frequency and magnitude of external agents.

This article has been accepted for publication and undergone full peer review but has not been through the copyediting, typesetting, pagination and proofreading process which may lead to differences between this version and the Version of Record. Please cite this article as doi: 10.1002/2016JF003975

© 2016 American Geophysical Union. All rights reserved.

1. INTRODUCTION

Located at the interface between marine and terrestrial environments, salt marshes are ecosystem-based flood defenses that help reduce the impact of storms and hurricanes on coastal communities [e.g. Temmerman et al., 2013; Möller et al., 1999; Möller, 2006; Chen et al., 2011; Zhao and Chen, 2013]. In recent years, these vegetated surfaces have been at the center of many restoration projects based on the concept of "living shorelines" [e.g. Temmerman et al., 2013; Fagherazzi, 2014]. The value of their storm-protection services has been estimated up to 5 million USD per km^2 in the United States [e.g. Costanza et al., 2008], and 786 million GBP per year for the UK marshes [UK National Ecosystem assessment, 2011; Foster et al., 2013; Möller et al., 2014] . Salt marshes also provide other important ecosystem services such as nutrient removal, habitat provision, and carbon sequestration over decennial to millennial time scales [e.g. Plater et al., 1999; Zedler and Kercher, 2005; Mudd et al., 2009]. Large salt marsh losses have been documented world-wide; as an example, in England and Wales salt marsh areal loss has been estimated to be around 83 ha per year by the UK Environmental Agency [Foster et al., 2013; Environmental Agency, 2011], 105 ha per year for the period in between 1993 and 2013 [Pye and French, 1993], and 349 ha per year for the period between 1998 and 2048 [Lee, 2001]. In the Solent, (UK), 40 % of the total area present in 1971 was eroded between 1971 and 2001 [Cope et al., 2008], while for the Greater Thames the erosion was estimated to be around 25 % of the total area present in 1973 [Cooper et al., 2001]. For areas in the south west of the Netherlands and the Wadden Sea, cliff erosion up to 4 m/yr has been recorded, despite positive vertical accretion rates [e.g. Bakker et al., 1993].

© 2016 American Geophysical Union. All rights reserved.

For the Southern part of the Venice Lagoon and for an area of 50 x 50 m, marsh edge retreat has been estimated around 1.2-2.2 m/yr for the period from 1993 to 1995. Highly dynamic patterns in marsh change have been identified, with accretion rates varying from 1.1 to 2.3 cm/yr [Day et al., 1998]. Highest accretion rates corresponded to the occurrence of strong storms as a consequence of sediment resuspension from nearby tidal flats. Day et al. [1998] suggested that this area was rapidly deteriorating due to lateral migration exceeding vertical accretion.

Erosion rates with similar order of magnitude and up to 80 cm/yr have been recently measured in the Northern part of the Venice Lagoon [e.g. Bendoni et al., 2016], where it has been also shown that failures of large marsh blocks do not necessarily correlate with instantaneous wave forcing, and that such large failures can also occur during calm periods. For the East Coast of the United States, long term field measurements of salt marsh erosion in Plum Island Sound and Virginia Coast Reserve [Leonardi et al., 2014, 2015] also demonstrated that failures of large marsh blocks can happen independently from high wave energy conditions. High resolution field data also suggest that salt marsh erosion is more spatially variable in case of low wave energy conditions, rather than under high wave energy, and that under low wave energy conditions erosion events follow a long-tailed frequency-magnitude distribution [Leonardi et al., 2014, 2015].

Salt marsh resistance to external agents is linked to sediment dynamics as well. For instance, measurements in the Wadden Sea [Schuerch et al., 2014], as well as numerical and field experiments in the Scheldt estuary [Temmerman et al., 2003] indicate that salt marsh erosion or accretion depends on the exchange of sediments between salt marshes, tidal flats, and tidal channels. Vegetated surface also influence salt marsh erosion by indirectly modifying soil parameters [e.g. Feagin et al., 2009].

© 2016 American Geophysical Union. All rights reserved.

In terms of vertical dynamics, salt marsh accretion rates have been found to be spatially and temporally variable [e.g. Day et al., 1998; Temmerman et al., 2004; Pethick, 1993]. Variability in accretion rates has been identified as largely depending on the proximity of tidal channels, erosion rates of nearby areas, as well as tidal flat characteristics [Day et al., 1998; Mariotti et al., 2014; Temmerman et al., 2004, 2005]. As an example, salt marshes in the southeast England have been found to more rapidly accrete right behind the erosional front [e.g. Day et al., 1998]. In spite of accretion rates being spatially variable, numerous studies confirm that feedbacks between sediment deposition, organic matter accretion, and biomass production generally allow salt marshes to be stable on the vertical direction and keep pace with sea level rise [e.g. Cundy and Croudace, 1996; van der Wal and Pye, 2004; Temmerman et al., 2003, 2005; Temmerman and Kirwan, 2015; Kirwan et al., 2016]. While resistant to sea level rise, salt marshes are inherently weak and vulnerable to lateral erosion induced by wave action because wind waves impact bare sediments below the vegetated surface where material is easily mobilized [e.g. Schwimmer, 2001; van de Koppel et al., 2005; Marani et al., 2011; McLoughlin et al., 2015; Fagherazzi, 2013; Leonardi et al., 2016].

Because wind waves are one of the main agents contributing to marsh lateral erosion, understanding their action is critical for restoration projects aimed at the maintenance and improvement of wetland ecosystem services.

Salt marsh erosion by wind waves is a complex phenomenon that includes several mechanisms such as the continuous removal of small particle aggregates from the marsh platform and marsh edges or the sudden and discontinuous detachment of marsh portions having size comparable to the bank height [e.g. Winterwerp and van Kesteren, 2004; Bendoni et al., 2013]. For example, waves can undercut the root mat with the formation of a marsh overhang that eventually breaks off and topple [e.g. Schwimmer, 2001; Allen, 1989]. For salt

© 2016 American Geophysical Union. All rights reserved.

marshes, downward shearing, bending followed by tensile fractures, and suborizontal tensile fractures are common failures mechanisms as well [e.g. Allen et al., 1989].

Herein, we will use the term "erosion event" to refer to the erosion rate (m/y) along relatively short marsh portions (i.e. stretches of shoreline of the order of 3 m), and that might be caused by continuous particle removal, mass failures or by a combination of both.

A direct relationship between wave energy and salt marsh lateral retreat has been recognized in prior studies [e.g. Schwimmer 2001; Marani et al., 2011; McLoughlin et al., 2015]. However, many existing studies only focus on small spatial scales (shoreline lengths of the order of hundreds of meters), and less attention has been paid to the uniformity of salt marsh erosion along stretches of shorelines at a bay or estuary-scale, as well as to the possible influence of different wind wave exposures and erosion rates on the shape of marsh boundaries.

Studies of erosion rate uniformity along marsh boundaries are relevant to the risk assessment of coastal wetlands, as they provide information about the occurrence of erosion events far from the average. In fact, the occurrence of unexpected erosion episodes raises questions about the effectiveness of risk assessment plans and coastal protection schemes. There is, thus, a need to further understand the occurrence of infrequent episodes, and whether they might be different from average, long-term erosion trends [Malamud, 2004; Bernardare et al., 2008; Leonardi et al., 2015]. The occurrence of isolated large erosion events could lead to inaccurate evaluations of the erosion trends in the area if detailed datasets for the morphological behavior of salt marshes or detailed surveys of the region are not present. It is thus appropriate to distinguish erosion rates averaged over large spatial scales with respect to localized erosion rates.

© 2016 American Geophysical Union. All rights reserved.

Many studies use wave power as a proxy for wind wave exposure [e.g. Schwimmer, 2001; Marani et al., 2011]. While this approach has been successful, wave thrust (integral along the vertical of the dynamic pressure) could be another useful indicator for the action of wind waves on wetland boundaries because it represents the actual force contributing to the dynamic equilibrium of marsh shorelines [e.g. Tonelli et al., 2011; Bendoni et al., 2014; Francalanci et al., 2013], and allows taking into account the presence of different water levels and marsh boundary features such as platform elevation with respect to mean sea level, and orientation of the boundary with respect to wave direction.

Water levels have been found to influence the action of wind waves [e.g. Tonelli et al., 2010; Möller et al., 1999, 2014; Möller, 2006]; laboratory, numerical and field experiments [e.g. Tonelli et al., 2010; Bendoni et al., 2014; Francalanci et al., 2013] confirm that the erosive action of wind waves at the edge of salt marshes is more severe when water levels are slightly below the marsh platform. Specifically, wave action has been found to increase with water depth, up to the point when the marsh is submerged, and then it rapidly decreases. When the wave peak is lower than the marsh platform, waves are partially reflected, interfering with incident waves. Once the bank is submerged, wind waves are affected by the water depth on the marsh platform. In these conditions waves rapidly break, and a large amount of energy is dissipated due to the presence of vegetation [e.g. Le Hir et al., 2000; Möller et al., 1999; Möller, 2006; Temmermann et al., 2005]. For very high water levels skimming flow may take place across a completely submerged canopy reducing wave energy dissipation. However, at these high water depths the wave thrust on the marsh boundary is minimal, leading to limited marsh erosion [Tonelli et al., 2010]. Wave thrust calculation is also fundamental to physically based models aimed at describing specific failure mechanisms such as block toppling. For the latter, marsh blocks are schematized as rigid and subject to hydrodynamic forces, gravity, and soil cohesion [e.g. Bendoni et al., 2014, 2016; Francalanci et al., 2013]. It is therefore

© 2016 American Geophysical Union. All rights reserved.

appropriate to test the suitability of more physically based parameters to describe marsh erosion, as the base to gradually incorporate specific failure mechanisms into numerical studies.

In this manuscript we focus on erosion processes and wave action at the boundary of salt marshes in the Barnegat Bay-Little Egg Harbor system using aerial images and a numerical model. We focus on the spatial distribution of lateral erosion rates and on the relationship between the shape of marsh boundaries and erosion rates. Fractal dimension is used as an indicator for the shape of marsh boundaries. We explore whether marsh boundary geometry can be used to infer whether salt marshes are slowly or rapidly degrading. To this end, an erosion analysis has been carried out for extensive stretches of shoreline (order of hundreds of kilometers). We further explore the long-term relationship between erosion rates and wave thrust at the marsh boundary. The analysis of marsh boundary geometry builds on previous work conducted on other salt marshes in the Unites States Atlantic Coast, and according to which a relationship exists between marsh boundary roughness and wave energy [Leonardi and Fagherazzi, 2014, 2015]. The second part of the work builds on numerous studies according to which there is a strict relationship between salt marsh erosion rates and wave energy [Schwimmer et al., 2001; Marani et al., 2011; Leonardi et al., 2016].

© 2016 American Geophysical Union. All rights reserved.

2. STUDY SITE

The Barnegat-Bay-Little Egg Harbor system is located along the central New Jersey coastline in Ocean County on the eastern seaboard of the USA (Figure 1), and consists of three shallow coastal bays: Barnegat Bay, Manahawkin Bay, and Little Egg Harbor. The system is comprised of a shallow, lagoon type estuary, separated from the Atlantic Ocean by a narrow barrier island complex approximately 70 km long.

The width of the lagoons ranges from 2 to 6 km, and the water depths range from 1 to 5 m, with an average value of 1.5 m. Most of the western side of Barnegat Bay is deeper (~1-3 m depth) than the Eastern side (~1 m depth). The deepest area runs along the Intracoastal Waterway and spans the bay length [Kennish, 2001; Defne et al., 2014; Aretxabaleta et al., 2014]. The barrier is breached at Barnegat Inlet and Little Egg Inlet. Barnegat Inlet has a mean width of 400 m, and a maximum water depth of 15 m. Little Egg Inlet has a width of approximately 2 km, and average water depth of 10 m. Figure 1 shows the bathymetry of the area and long-term statistics of hourly mean wind speed and direction (period from 1991-2013).

During the fall and winter seasons winds predominantly come from northwest to west directions; during spring and summer the jet stream retreats northward and winds are from the south to the southwest; in summer subtropical high pressures generally produce warm and humid southerly breezes and average wind speed are less than 15 km/hr. The area is also characterized by northeasterly winds coming from coastal low pressure storms (Nor'easters) which move toward the north along the coast. These extratropical storms occur from September to March. In summer, thunderstorms are frequent. Late summer and fall can be characterized by the occurrence of hurricanes, and tropical storms. Generally, the frequency with which major hurricanes impact the area is lower with respect to more southerly Atlantic states. For Barnegat Bay and nearby areas, on average, one tropical cyclone passes within

© 2016 American Geophysical Union. All rights reserved.

100 km from the coast every 4.5 years [Kennish, 2001; Elsner, J.B. and Kara, 1999]. As an example, between 1935 and 1967 nine hurricanes occurred within 160 km from the Bay [Kennish, 2001; U.S. Atomic Energy commission, 1974]. Extratropical coastal storms (Nor'easters) are more frequent in the area. Because Nor'easters winds have usually wind velocity lower than hurricanes, their damage is generally restricted to the coast, while hurricanes damage can extend inland significantly. On the other hand, since Nor'easters are large, their damage can cover extensive coastal areas [Elsner, J.B. and Kara, 1999].

Wind measurements were used to reconstruct the wave climate in the area. In enclosed basins like the one studied herein where waves are locally generated, it is realistic to assume that waves instantaneously adjust their direction to the wind direction [Mariotti et al 2010]. Tides are semidiurnal, the tidal range outside the Bay is over 1 m, but it attenuates within the estuary to less than 20 cm in some locations [Aretxabaleta et al., 2014]. In the past, the lagoon was almost completely fringed by salt marshes. In 1888, the salt marsh area was approximately 14850 ha, while in 1995 the marsh extent was estimated to be 9940 ha; this decline has been attributed to both natural and human disturbances, such as land use change and dredging operations [Lathrop and Bognar, 2001]. Lower marsh areas are covered with the short form of *Spartina alterniflora*, while the high marsh is covered with *Spartina patens* [Suk et al., 1999]. Vegetation characteristics can be important when dealing with erosion, as vegetation can trap sediments trough leaves and promote sedimentation rates, slow the flow, increase soil resistance trough the root mat, promote certain type of marsh failures (e.g. root mat toppling) with respect to other failure mechanisms, and influence soil properties [e.g. Feagin et al., 2009; Moeller, 2006]. Among others, species zonation, vegetation density, stem height, and Young's modulus can significantly influence frictional resistance [e.g. Allen et al., 1992]. To characterize vegetation friction, many studies have focused on the overall roughness coefficient of vegetation by using a variety of laboratory, field and numerical

© 2016 American Geophysical Union. All rights reserved.

methods [e.g. Kouwen and Li, 1980; Tsujimoto et al., 1996; Jarvela, 2002]. Other studies have been focusing on the effect of vegetation on flow resistance with artificial plants or by schematizing stems as rigid cylinders. These studies have used a variety of laboratory and numerical techniques [e.g. Nepf 1999, 2012]. Real plants have been also used to directly investigate frictional resistance trough field and laboratory experiments [e.g. Jarvela, 2002; Armanini et al., 2005; Allen et al., 1992].

3. METHODS

3.1 Aerial photography

To determine the geometry of salt marsh boundaries and related erosion rates at a large spatial scale we used a suite of aerial images (1930, 1995, 2002, 2007, 2010, 2013). For the 1930, 2007, and 2013 aerial photographs, we digitized more than 100 km of marsh shoreline, corresponding to the majority of the interior marsh boundary. Using the digitized aerial images, we then computed salt marsh erosion from 1930 to 2013 and from 2007 to 2013 (Figure 2, 3). The three aerial images were selected among the available ones based on their quality, and with the aim to investigate long-term erosion rates (1930-2013), as well as more recent and shorter-term rates of change (2007-2013). Specifically, images for 1930 and 2013 were the farthest available in time, and the period from 2007 to 2013 was the shortest interval at which changes in marsh edges profile were still detectable for the majority of the shoreline. For the 1995, 2002, and 2010 images we digitized a series of 10 small marsh shoreline portions of the order of 1 km to retrieve information about erosion at a higher temporal resolution (Figure 3a). The 1930 image is a black and white aerial photograph produced by scanning 261 mosaic tile prints at 400 dpi, with an average pixel size of 1.98 m, and 24.3 m RMS. The 2002 and 2007 images are respectively infrared and natural color orthophotographs produced at a scale of 1:2400 with a 0.3 m pixel resolution. The average

© 2016 American Geophysical Union. All rights reserved.

horizontal accuracy is ±1.2 m with a 95 % confidence level. The 1995, 2010, and 2013 natural color orthophotographs were obtained by using 1 m ground sample distance (GSD) source images and were rectified with an average horizontal accuracy of ±5 meters with a 95% confidence level. Images for 1995, 2002, 2007, 2010, and 2013 were obtained in their orthorectified form, and did not require particular post-processing. The 1930 photograph was rectified using georeferencing tools within ArcGIS®, and by considering as ground control points within different tiles, corner of buildings and road intersections. The mean root-mean-square error of the 1930 aerial photograph rectifications was ±5 m. The wetland boundary was digitized by contouring the shoreline through ArcGIS® points features placed at an average distance of 2.5 m. The total position uncertainty, U_t, was estimated following established methodologies [e.g. Genz et al., 2007; Fletcher et al., 2003; Cowart et al., 2011], and by accounting for both rectification (E_r) and digitalization (E_d) errors.

$$U_t = \pm\sqrt{\Sigma {E_r}^2 + \Sigma {E_{di}}^2} \quad (1)$$

where the sum refers to all used images. A digitalization error, E_i, of 0.5 m was calculated by digitalizing same stretches of shorelines multiple times and finding the maximum distance between multiple digitalizations. Maximum position uncertainties (U_t), are 24.8 m for the comparison of 1930-2007 and 25.33 m for the 1930-2013 image comparison, which correspond to a maximum uncertainty of 0.32 m/y, and 0.30 m/y respectively. Given two tracked shorelines, at every point along the first boundary, erosion was estimated as the minimum distance of that point from points belonging to the shoreline of the other year.

To compute shoreline fractal dimension, we followed the Minkowski–Bouligand method [e.g. Dubuc et al., 1989]. Fractal dimension allows evaluating the degree of marsh boundary complexity by computing how fast length measurements change with the scale at which they are measured. Generally speaking, given a topological set S of dimension n, for any small

© 2016 American Geophysical Union. All rights reserved.

value $\varepsilon > 0$, let $N_\varepsilon(S)$ be the minimum number of n-dimensional cubes of side-length ε needed to cover S. The fractal dimension, D, is such that:

$$N_\varepsilon(S) \sim 1/\varepsilon^D \text{ as } \varepsilon \to 0 \tag{2}$$

and:

$$D = -\lim_{\varepsilon \to 0} \frac{\log N_\varepsilon(S)}{\log(\varepsilon)} \tag{3}$$

When approaching the limit, if the surface is smooth and differentiable, its fractal dimension, D, equals the topological dimension, d. For a rough and non-differentiable curve the fractal dimension may exceed the topological dimension d.

We are also interested in evaluating the frequency-magnitude distribution of erosion events. In particular, it is useful to have information about the possible occurrence of unexpected and above average erosion rates that belong to the tail of the erosion events distribution. To gain more information about these tail events, we approximate the frequency-magnitude distribution of erosion events by means of a logarithmic frequency-magnitude distribution. The main advantages of using a distribution that is normal in the logarithm of a parameter are: i) the distribution is positive-definite, and it is thus suitable to represent quantities that cannot be negative, such as erosion rate values; ii) for many natural processes, where the possibility of events falling far from the average exists, a logarithmic distribution often provides a better fit with respect to Gaussian-like functions [.g. Limpert et al., 2001].

For a log-normal distribution, the probability density function, f_x is:

$$f_x(x, \mu, \sigma) = \frac{1}{x\sigma\sqrt{2\pi}} e^{-\frac{(lnx-\mu)^2}{2\sigma^2}} \tag{4}$$

© 2016 American Geophysical Union. All rights reserved.

Where μ is the mean, and σ is the variance. With increasing variance, the tail of the distribution of erosion events gets longer, distribution skewness increases, and the possibility of erosion events far from the mean increases as well.

3.2 Numerical Model

In this study we used the Coupled-Ocean-Atmosphere-Wave-Sediment-Transport (COAWST) Modeling System [Warner et al., 2008; Warner et al., 2010]. In COAWST, the ocean model ROMS, atmospheric model WRF, wave model SWAN, and modules of the Community Sediment Transport Model are fully coupled by means of the Model Coupling Toolkit. The ocean model ROMS is a three-dimensional, free-surface, terrain-following model solving finite difference approximations of the Reynolds Averaged Navier-Stokes equations, using hydrostatic and Boussinesq assumptions [Chassignet et al., 2000; Shchepetkin and McWilliams, 2005; Haidvogel et al., 2008; Kumar et al., 2011]. To include the effect of surface waves, the momentum equations require, as input, information for wave height, wave energy dissipation, propagation direction, and wavelength. These information are obtained from the numerical model SWAN (Simulating Waves Nearshore), which solves the transport equations for waves action density, and accounts for shoaling, refraction, wind waves generation, wave breaking, bottom dissipation, and non-linear wave interactions [Booij et al., 1999; Ris et al., 1999].

The boundaries of the model domain are presented in Figure 1A (yellow line) and include Barnegat Bay, Little Egg Harbor, part of Great Bay to the South, and Manasquan Inlet to the north. The computational grid consists of 160 East-West and 800 North-South grid points with seven vertical layers having equal depth. Cell sizes vary from 40 to 200 m, with the grid being refined at the inlets and around complex morphological features. The bathymetry is based on the National Ocean Service Hydrographic Survey data [NOAA NOS 2012, Defne

© 2016 American Geophysical Union. All rights reserved.

and Ganju, 2014]. At the seaward boundaries, we prescribed water level variations typical of a tidal cycle based on the ADCIRC tidal constituents database for the North Atlantic Ocean, and used a combination of Flather and Chapman boundary conditions. The Flather [Flather, 1976] boundary condition allows radiating out deviations of the normal component of baratropic velocities at the speed of external gravity waves, and the Chapman boundary condition is the corresponding condition for surface elevations [Chapman, 1985]. At the westward boundary we prescribed a radiation boundary condition following Orlanski [1976] radiation scheme, and allowing tidal energy to propagate landward. The model was calibrated by changing the bottom roughness coefficient to attain the best agreement with measurements from 7 water level stations and 3 tidal discharge stations of the US Geological Survey within the Barnegat Bay Little Egg Harbor estuary and for a period comprising the first two weeks of March 2012. The Brier-Skill-Score [e.g. Murphy and Epstein 1989] was used to assess model calibration. Skill assessments of the model ranged from very good to excellent [Defne and Ganju, 2014]. More specific information about the model as well as model calibration and setup can be found in Defne and Ganju [2014]. The model was run with constant wind speed and direction using 3 classes of wind (5 m/s, 10 m/s, and 25 m/s), 8 directions spanning from 0 to 360°, and 4 different storm surge values (+-0.3m and +- 1m), for a total of 96 simulations. Results obtained from these simulations were combined with wind speed, wind direction, and water level data retrieved from a nearby NOAA station (station ID LLNR 830, 40°15'3" N 73°9'52" W) to get a proxy for the long term wave climate along the shoreline. We obtained the model outputs indicated above by using the phase averaged model SWAN to calculate wave parameters along marsh boundaries, and then followed results from a phase resolving model [Tonelli et al., 2010] to evaluate the reduction in wave thrust occurring when waves overtop the marsh scarp. The model proposed by Tonelli et al., [2010] combines non-hydrostatic Boussinesq equations, nondispersive nonlinear shallow water equations, and has

© 2016 American Geophysical Union. All rights reserved.

been widely validated. Results presented by Tonelli et al., [2010], and used in this manuscript focus on areas of the marsh platform close to the marsh edge (1-3 m), and incorporate the presence of vegetation through the use of friction factors typically derived for salt marshes (0.07-0.47; Department of the Army, Waterway s Experiment Station, Corps of Engineers, and Coastal Engineering Research Center [1984]). Wave thrust is calculated as the integral along the vertical axis of the dynamic pressure of waves. The dynamic pressure of wind waves can be calculated as:

$$p_d(z,t) = \rho g K_p(z)\eta(t) \tag{5}$$

where $K_p(z)$ is the pressure-response factor accounting for the dynamic component due to water particle acceleration, and can be calculated as:

$$K_p(z) = \frac{\cosh k(h+z)}{\cos(kh)} \tag{6}$$

To take into account the dependence of wave thrust on water depth, we followed results from Tonelli et al. [2010], and prescribed an up to 60% linear reduction in wave thrust proportional to the water depth on the marsh platform up to 0.4 m above the surface, after which wave thrust is kept constant. As part of this project we also developed a subroutine for wave thrust calculation, which is now implemented in the COAWST modeling suite (see supplementary material).

This is a simplified approach, and present several limitations particularly in regard to the dissipative effect of vegetation which might strongly change depending on both vegetation and wave characteristics. Vegetation properties can be especially important: trough wave flume experiments it has been shown that, over a distance of 40 meters, up to 60 % of

© 2016 American Geophysical Union. All rights reserved.

dissipation is attributable to the vegetation cover even under extreme storm conditions [Möller et al., 2014; Möller, 2006]. Similar conclusions have been drawn from field measurements, according to which wave energy dissipation up to 63% was found to occur over the first 100 meters [Möller et al., 1999; Brampton 1992]. Variable dissipation rates have been measured in the field [e.g. Koch 1996; Prager and Halley 1999] and an exponential energy decay with respect to the distance of the shoreline has been generally accepted with exponents of the order of 0.0187 [e.g. Brampton et al., 1992; Möller et al., 1999]. This simplified approach is herein accepted in part for the lack of direct field measurements of waves over vegetated surfaces, and in part because we are focusing on the action of waves at the edges of the marsh boundary. Over such short distances (1-3 m) the action of vegetation is not fully developed even if an exponential formulation for wave energy dissipation over distance is assumed [Tonelli et al., 2011; Möller et al., 1999].

4 RESULTS

4.1 Boundary erosion analysis

Figure 2b,c reports fractions of the entire shoreline subject to different erosion rates and presents an overview of the long term (1930-2007) erosion rate, with respect to more recent and short-term erosion rate values (2007-2013). Percentages refer to the entire digitized shoreline. For both time intervals, more than half of the digitized shoreline is eroding at rates ranging from 0.25 to 2 m/y. Around 25 % of the shoreline is eroding slower than 0.25 m/yr, or is not eroding at all. For both periods erosion rates are similar and reach a maximum near Little Egg Harbor. Despite small percentage differences among different erosion categories, no substantial variations can be noticed when comparing average long-term and short-term erosion rates at a large spatial scale.

© 2016 American Geophysical Union. All rights reserved.

Spatial variations in erosion rate for the period 1930-2007 are presented in Figure 3. The highest erosion rates occur in proximity of Little Egg Inlet, around points of greatest fetch in Little Egg Harbor, and in the western part of Barnegat Bay. Figure 3b shows variation in erosion rate with respect to the alongshore distance from the shoreline. The horizontal coordinate follows the white arrows of panel A. Blue, and red lines are long- (1930-2007), and short- term (2007-2013) erosion rates respectively. Yellow and cyan lines are corresponding averages over moving distances of 1 km. Despite the measurement noise, the erosion rates for the two periods maintain a similar trend for most of the marsh boundary, in terms of both magnitude and spatial distribution (Figure 4a). Strongest differences occur for points around Little Egg Inlet, where the erosion rate is one of the highest within the domain, but has lowered in the period 2007-2013 with respect to the period 1930-2007. To better highlight possible temporal variations, erosion rates for shorter intervals of time are presented in Figure 4B for 10 different stretches of shoreline having an average length of 1 km. Apart from locations in proximity of Little Egg inlet, erosion rates remain similar in time, and mainly oscillate around a constant value.

Fractal dimension was used to estimate shoreline roughness, and the existence of a potential relationship between erosion rate and morphology of salt marsh boundaries. Figure 5A, C show the relationship between the fractal dimension of the marsh boundary and erosion rates for the period from 1930 to 2007, and from 2007 to 2013 respectively. Fractal dimension is significantly ($p<0.05$) and negatively correlated to erosion rate, suggesting that rapidly eroding areas have smoother marsh boundaries with respect to slowly eroding areas.

To gain further information about salt marsh erosion processes it is useful to investigate the frequency magnitude distribution of erosion events. The likelihood of an erosion event to deviate from average erosion rates was estimated by approximating the frequency-magnitude distribution of erosion events using a log-normal distribution, and by computing

© 2016 American Geophysical Union. All rights reserved.

corresponding standard deviation values. The log-normal standard deviation is negatively correlated to average erosion rates (Figure 5b,d). This result indicates that unexpected erosion rates far from the mean occur more often in slowly eroding areas. On the contrary, low standard deviation values, corresponding to high average erosion rates, indicate that in rapidly degrading marshes the majority of erosion episodes fall around the mean. Figures 5e, f, g provide examples of frequency magnitude distributions of erosion events and marsh boundary profiles at three different sites. Site locations are indicated in Figure 3 (numbering in Figure 5c, d, e corresponds to numbering in Figure 3a). It is possible to notice that a long tail of the frequency-magnitude distribution of erosion events corresponds to a slowly eroding marsh with a rough boundary.

4.2 Wind-wave exposure analysis

Figure 6 represents long-term (1991-2013) average wave thrust values calculated at marsh boundaries for the entire bay. Wave thrust values in Figure 6 correspond to values averaged throughout a tidal cycle, and then further averaged from 1991 to 2013. Herein results refer to the period from 1991 to 2013 because no wind data before 1991 are available from buoy stations. Wave thrust values along the boundary were obtained by associating at every point of the boundary and for every wind speed, direction, and water level, wave thrust values obtained from the numerical tests carried out to assess general system susceptibility to different winds and water levels. If a reduction in wave thrust for a submerged marsh is taken into account (Figure 6b), average wave thrust values for the period of interest strongly decline but maintain a similar spatial distribution. Some differences in the spatial distribution of the two different wave thrust calculations are present at the north-eastern corner of Great Bay, and at the west side of Barnegat Bay. Generally speaking, the eastern part of Barnegat

© 2016 American Geophysical Union. All rights reserved.

Bay, the southeast side of Great Bay, and points of greatest fetch in Little Egg Harbor appear to be the most exposed to the action of wind waves.

Figure 7a shows the relationship between wave thrust and salt marsh erosion rates. Wave thrust values refer to the 1991-2013 period, while erosion rates values refer to the 1930-2013 period. These time frames are meant to represent long-term averages for both wave thrust and erosion rates. The time frame limitation for wave thrust values is connected to wind data availability. We retain that the comparison is acceptable because it spans relatively long temporal intervals, and because it has been previously shown that for the majority of the shoreline erosion rates maintain a similar trend in time. Figure 7b, c, and d represent the same relationship but for three different salt marsh categories: mainland marshes, likely characterized by muddy substrates [Kennish 2001], back-barrier marshes, displaying thin sand deposits driven by storms for some distance into the marshes [Fisher 1961], and marshes with abundance of ponds [Elsey-Quirk and Adamowicz 2016]. The latter category was chosen based on results suggesting the importance of marsh ponds for marsh deterioration [e.g. Mariotti et al., 2012]. In some marshes of Barnegat Bay the number of ponds was artificially increased by Open Marsh Water Management (OMWM), a technique introduced for mosquito control. Recent studies show that marsh area with pools and ponds have less sediment deposition and less surface accretion, while being on average higher [Elsey-Quirk and Adamowicz 2016]. Each cell of the grid used for the computation of wave thrust contains multiple digitization points and erosion rates. For this reason, when comparing wave thrust and erosion rates, data have been binned. Each point in the panel represents average wave thrust and erosion rate for a given bin. Each grey line is the standard deviation for that bin. Binning has been done every 40 points which is the average number of digitalization points per grid cell. When comparing wave thrust, and erosion rate for a specific marsh category (e.g. back-barrier marshes or marsh with ponds, Figure 7b,c, and d),

© 2016 American Geophysical Union. All rights reserved.

we first isolated the data belonging to each marsh category, and then we binned the data using the same number of bins than for Figure 7a. Despite the noticeable scatter, wave thrust and salt marsh erosion rates are significantly correlated for each salt marsh category. The best fit occurs when all marshes are considered together. Scatter might arise from a variety of other sources. Among others, differences in vegetation density, bioturbation, and land use might significantly affect salt marsh erosion rates [Feagin et al., 2009; Paramor and Hughes, 2004]. Scatter might also arise from heterogeneneities in sediment substrate caused by the intermittent presence of overwash sand layers likely causes a large scatter in soil resistance and erosion rates.

5. DISCUSSION

From a long-term analysis of salt marsh lateral retreat in the Barnegat Bay and Little-Egg Harbor system, we show that no drastic temporal variations in salt marsh erosion rates are present. Specifically, for the majority of the digitized shoreline, erosion rates evaluated for the period from 1930 to 2007 are similar and of the same order of magnitude of erosion rates that took place from 2007 to 2013. Same results are obtained when considering smaller stretches of marsh boundary and shorter time intervals. Erosion rate appears constant for the majority of the locations taken into account. Points around Little-Egg Inlet are the only locations where a different decrease in erosion rate has occurred. This difference might be due to changes in land use, and coastal restoration practices adopted in the area [Psuty and Ofiara, 2002]. As an example, before 1950 no buildings were present in close proximity to the shoreline, while nowadays areas between Barnegat Inlet and Little Egg inlet are highly developed. Many locations along the barrier island are interested by both soft and hard engineering structures such as groins and jetties exerting shadow effects on the longshore drift which is predominantly to the south [Psuty, and Ofiara, 2002]. Beach nourishment also

© 2016 American Geophysical Union. All rights reserved.

occurred in the area. For instance, the entire barrier island received beach nourishment in 1962-63 after the Ash Wednesday Northeaster; during the 1990s beach nourishment projects were also carried out in areas south from Barnegat Inlet up to Brant Beach [Psuty and Ofiara, 2002]. Generally, the southern barrier island edges around Little Egg Inlet have significantly expanded; this could have helped protecting the interior part of the salt marsh peninsula where erosion rates have been declining.

According to Figure 4b, erosion rates for the 2007-2010 period are of the same order of magnitude of the rates for the 2010-2013 period. This is especially relevant considering that the second period (2010-2013) was characterized by the occurrence of Hurricane Irene and Hurricane Sandy. Differently from the storms in 2007-2010 that only passed near the area, both Irene and Sandy made landfall in New Jersey, and are the only storms in record that caused hurricane force wind in our study area. Both storms caused damages, and the latter is considered as the most destructive in the history of New Jersey [e.g. Blake et al., 2012; National Hurricane Center; see also Figure S1]. Specifically, Sandy was ranked as 1/900 year event, and the return period for the storm surge has been estimated to be 1570 years, based on generalized extreme value return curves [Brandon et al., 2014]. In fact, Hurricane Sandy crossed the New Jersey coastline at an angle closer to 90 degrees than any other hurricane in record [Figure S1]. This was caused by a combination of a blocking high pressure over the western North Atlantic and the interaction with an extratropical upper level disturbance [Holl and Sobel, 2013].

For the area of interest, extreme erosion of salt marshes did not happen in spite of the two large storms. This could be connected to the fact that once a salt marsh is submerged, wave action significantly decreases due to wave energy dissipation above marsh surfaces [e.g. Tonelli et al., 2010; Chen et al., 2011; Moller et al., 2014]. For instance, even if the storm surge associated with Hurricane Sandy caused severe damages to the open coast (for example

© 2016 American Geophysical Union. All rights reserved.

to sandy beaches, Figure S1), the presence of a high storm surge might have reduced wave impact on salt marshes which are more vulnerable when the water level is around mean sea level. This is in agreement with results presented in Leonardi et al., [2016] showing in terms of geomorphic work that salt marsh erosion is dictated by average weather conditions (gentle to fresh breeze according to Beaufort wind scale) rather than strong storms. Our findings are also supported by recent results showing high temporal resolution field measurements of salt marsh erosion collected in the Venice Lagoon every month for 1.5 years, at six different locations [Bendoni et al., 2016]. According to these surveys, erosion remains constant in time, and such that the cumulative erosion profile has constant gradient [Bendoni et al., 2016].

For the Barnegat Bay area, the late Holocene relative sea-level rise has been around 1.3±0.2 mm/yr [Engelhart et al., 2009]. While this could have affected erosion rates, there is extensive evidence that salt marshes are able to keep peace with sea level rise and maintain their elevation constant with respect to mean sea level thanks to their relatively high accretion rates [e.g. Day et al., 1998; Fagherazzi, 2013; Fagherazzi et al., 2013 Kirwan et al., 2008, 2009, 2010, 2013, 2016; Mariotti et al., 2013 and many others]. Elsey-Quirk and Adamowicz [2016] measured accretion rates of 1.8 ± 0.8 mm/year in the Bernagat Bay marshes, which partly offset sea-level rise. Herein we mainly focus on spatial variations in erosion rate within Barnegat Bay, and a deeper understanding of the role of sea-level rise in salt marsh decline is outside the scope of this work, as it might be difficult to infer differential erosional rates induced by sea level variations at a Bay scale.

The emergent relationship between salt marsh erosion and shoreline roughness suggests that the shape of marsh boundaries is a possible geomorphic signature of the magnitude of erosion events and wetland-vulnerability to wind waves. Specifically, while rough shorelines (high fractal dimension) correspond to slowly eroding salt marshes, smooth shorelines (low fractal

© 2016 American Geophysical Union. All rights reserved.

dimension) characterize rapidly degrading coastlines. The relationship between marsh boundary geometry and erosion rates is also recognizable from the frequency-magnitude distribution of erosion events. While rapidly eroding shorelines are characterized by a Gaussian frequency-magnitude distribution, slowly eroding shorelines display a logarithmic distribution. Similar results have been reported in Leonardi and Fagherazzi [2014, 2015] for salt marshes at other five locations in Massachusetts and in the Virginia Coast Reserve. By using field data and a cellular automata model, it has been shown that different geomorphic features emerge under high and low wave energy when natural heterogeneities (e.g. different soil properties, bioturbation, seepage erosion and many others) along marsh boundaries are taken into account. At low wave energy, the existence of a variability in erosional resistance causes differential erosion rates which in turn promote rough marsh boundaries and a long-tailed distribution of erosion events. On the contrary, high wave energy conditions correspond to a smooth marsh boundary and a Gaussian-like distribution of erosion episodes. For areas normally subject to low energy conditions, the occurrence of high energy events leads to boundary smoothing [Leonardi and Fagherazzi, 2015]. Variability in erosional resistance could be caused by several factors, such as vegetation cover, soil resistance, biological processes that are inevitably present along marsh shorelines [e.g. Feagin et al., 2009]. However, it has been shown that such emergent properties can be reproduced by just assuming randomly distributed resistance values and different wave energy conditions [Leonardi and Fagherazzi, 2014, 2015]. The understanding of the role played by salt marsh properties on salt marsh erosion would have benefitted from detailed field measurements of marsh resistance. These field measurements are not present in this manuscript, and this is a limitation that might be addressed in future studies.

© 2016 American Geophysical Union. All rights reserved.

Under a climate change scenario, a relationship between the erosion rate and the shape of marsh boundaries could be potentially used to infer changes in external agents, such as changes in mean wave climate or a change in the frequency of extreme events. This relationship can be also used to identify more vulnerable areas by visually evaluating the roughness of marsh boundaries.

6. CONCLUSIONS

We digitized more than 100 km of marsh shoreline and calculated salt marsh erosion rates for the Barnegat Bay and Little Egg Harbor system. We further computed shoreline fractal dimension, and the standard deviation of the erosion rates. Finally we correlated erosion rates to wave thrust values. Our analysis led to three main conclusions: i) for the majority of the shoreline, no drastic temporal changes in erosion rate have been observed. The spatial and temporal distribution of salt marsh erosion rates remained mostly unchanged ii) the magnitude of salt marsh erosion rate is recognizable from the morphology of the marsh boundary. Rapidly deteriorating salt marshes have relatively smooth marsh boundary profiles. On the contrary, slowly eroding salt marshes have been found to have rough marsh boundary profiles iii) we confirm the existence of a relationship between salt marsh erosion rate and wave energy exposure. Specifically, we found a significant correlation between wave thrust and shoreline change.

ACKNOWLEDGEMENT

This research was supported by the Department of the Interior Hurricane Sandy Recovery program (project GS2-2D) and by NSF DEB-0621014 (VCR-LTER program), OCE-1238212 (PIE-LTER program). We acknowledge the NJ Office of Information Technology (NJOIT), Office of Geographic Information Systems (OGIS) as the source of aerial images. The

© 2016 American Geophysical Union. All rights reserved.

numerical model COWAST is freely available for download at http://woodshole.er.usgs.gov/operations/modeling/COAWST/. We also thank Amer Suvalic for his contribution to shoreline digitization. We thank the editors and reviewers for their constructive and insightful comments.

REFERENCES

Allen, J.R.L., 1989. Evolution of salt-marsh cliffs in muddy and sandy systems: a qualitative comparison of British west-coast estuaries. Earth Surface Processes and Landforms, 14(1), pp.85-92.

Allen, J.R.L. and Pye, K., 1992. Coastal saltmarshes: their nature and importance. Salt Marshes, Morphodynamics, Conservation and Engineering Significance. Cambridge University Press, Cambridge, pp.1-18.

Aretxabaleta, A. L., B. Butman, and N. K. Ganju (2014), Water level response in back-barrier bays unchanged following Hurricane Sandy, Geophysical Research Letters, 41(9), 3163–3171, doi:10.1002/2014GL059957.

Armanini, A., Righetti, M. and Grisenti, P., 2005. Direct measurement of vegetation resistance in prototype scale. Journal of Hydraulic Research, 43(5), pp.481-487.

Bakker, Leeuw, Dijkema, Leendertse, Prins and Rozema, 1993 Salt marshes along the coast of the Netherlands.

Bendoni, M., S. Francalanci, L. Cappietti, and L. Solari (2014), On salt marshes retreat: Experiments and modeling toppling failures induced by wind waves, Journal of Geophysical Research: Earth Surface, 119(3), 603–620, doi:10.1002/2013JF002967.

Bendoni, M., Mel, R., Solari, L., Lanzoni, S., Francalanci, S. and Oumeraci, H., 2016. Insights into lateral marsh retreat mechanism through localized field measurements. Water Resources Research, 52(2), pp.1446-1464.

Bernardara, P., Schertzer, D., Sauquet, E., Tchiguirinskaia, I. and Lang, M., 2008. The flood probability distribution tail: how heavy is it?. Stochastic Environmental Research and Risk Assessment, 22(1), pp.107-122.

Blake E. S., Kimberlain T. B., Berg R. J., Cangialosi J. P. and Beven J. L. National Hurricane Center [http://www.nhc.noaa.gov/data/tcr/AL182012_Sandy.pdf]

Booij, N., R. C. Ris, and L. H. Holthuijsen (1999), A third-generation wave model for coastal regions: 1. Model description and validation, Journal of Geophysical Research: Oceans, 104(C4), 7649–7666, doi:10.1029/98JC02622.

Brandon, C. M., J. D. Woodruff, J. P. Donnelly, and R. M. Sullivan (2014), How Unique was Hurricane Sandy? Sedimentary Reconstructions of Extreme Flooding from New York Harbor, Sci. Rep., 4.

Brampton, A.H., 1992. Engineering significance of British saltmarshes. Saltmarshes: Morphodynamics, conservation and engineering significance, pp.115-122.

Chapman, D. C., 1985: Numerical treatment of cross-shelf open boundaries in a barotropic coastal ocean model, J. Phys. Oceanogr., 15, 1060--1075.

Chassignet, E. P., H. Arango, D. Dietrich, T. Ezer, M. Ghil, D. B. Haidvogel, C.-C. Ma, A. Mehra, A. M. Paiva, and Z. Sirkes (2000), DAMÉE-NAB: the base experiments, Dynamics of Atmospheres and Oceans, 32(3–4), 155–183, doi:http://dx.doi.org/10.1016/S0377-0265(00)00046-4.

© 2016 American Geophysical Union. All rights reserved.

Chen, Q., and H. Zhao (2011), Theoretical Models for Wave Energy Dissipation Caused by Vegetation, Journal of Engineering Mechanics, 138(2), 221–229, doi:10.1061/(ASCE)EM.1943-7889.0000318.

Costanza, R., O. Pérez-Maqueo, M. L. Martinez, P. Sutton, S. J. Anderson, and K. Mulder (2008), The Value of Coastal Wetlands for Hurricane Protection, AMBIO: A Journal of the Human Environment, 37(4), 241–248, doi:10.1579/0044-7447(2008)37[241:TVOCWF]2.0.CO;2.

Cowart, L., D. R. Corbett, and J. P. Walsh (2011), Shoreline Change along Sheltered Coastlines: Insights from the Neuse River Estuary, NC, USA, Remote Sensing, 3(7), 1516–1534, doi:10.3390/rs3071516.

Cooper, A., McCann, T., Rogers, D., 2009. Northern Ireland Countryside Survey 2007: Broad Habitat Change 1998e2007. Northern Ireland Environment Agency, Belfast.

Cope, S.N., Bradbury, A.P., Gorcznska, M., 2008. Solent Dynamic Coast Project: Main Report. New Forest District Council/Channel Coast Observatory.

Cundy, A.B. and Croudace, I.W., 1996. Sediment accretion and recent sea-level rise in the Solent, southern England: inferences from radiometric and geochemical studies. Estuarine, Coastal and Shelf Science, 43(4), pp.449-467.

Day, John W., Scarton Francesco, Rismondo Andrea, and Daniele Are. "Rapid Deterioration of a Salt Marsh in Venice Lagoon, Italy." Journal of Coastal Research 14, no. 2 (1998): 583-90. http://www.jstor.org/stable/4298811.

Defne, Z., and N. Ganju (2014), Quantifying the Residence Time and Flushing Characteristics of a Shallow, Back-Barrier Estuary: Application of Hydrodynamic and Particle Tracking Models, Estuaries and Coasts, 1–16, doi:10.1007/s12237-014-9885-3.

Department of the Army, Waterway s Experiment Station, Corps of Engineers, and Coastal Engineering Research Center (1984), Shore Protection Manual, vol. 1, 4th ed., 532 pp., Department of the Army, Waterways Experiment Station, Corps of Engineers, and Coastal Engineering Research Center, Washington, D. C.

Dubuc, B., J. F. Quiniou, C. Roques-Carmes, C. Tricot, and S. W. Zucker (1989), Evaluating the fractal dimension of profiles, Physical Review A, 39(3), 1500–1512.

Engelhart, S.E., Horton, B.P., Douglas, B.C., Peltier, W.R. and Törnqvist, T.E., 2009. Spatial variability of late Holocene and 20th century sea-level rise along the Atlantic coast of the United States. Geology, 37(12), pp.1115-1118.

Environment Agency, 2011. The Extent of Saltmarsh in England and Wales: 2006-2009. Environment Agency, Bristol.

Elsey-Quirk, Tracy, and Susan C. Adamowicz. "Influence of Physical Manipulations on Short-Term Salt Marsh Morphodynamics: Examples from the North and Mid-Atlantic Coast, USA." Estuaries and Coasts 39.2 (2016): 423-439.

Elsner, J.B. and Kara, A.B., 1999. Hurricanes of the North Atlantic: Climate and society. Oxford University Press.

Fagherazzi, S. (2013), The ephemeral life of a salt marsh, Geology , 41 (8), 943–944, doi:10.1130/focus082013.1.

Fagherazzi, S. (2014), Coastal processes: Storm-proofing with marshes, Nature Geosci, 7(10), 701–702.

Fagherazzi, S., G. Mariotti, P.L. Wiberg, and K.J. McGlathery. 2013. Marsh collapse does not require sea level rise. Oceanography 26(3):70–77, http://dx.doi.org/10.5670/oceanog.2013.47.

Feagin, R.A., Lozada-Bernard, S.M., Ravens, T.M., Möller, I., Yeager, K.M. and Baird, A.H., 2009. Does vegetation prevent wave erosion of salt marsh edges?. Proceedings of the National Academy of Sciences, 106(25), pp.10109-10113.

© 2016 American Geophysical Union. All rights reserved.

Fischer, A. G. 1961. Stratigraphic record of transgressing seas in light of sedimentation on Atlantic coast of New Jersey. AAPG Bulletin, 45(10), 1656-1666.
Flather, R. A., 1976: A tidal model of the northwest European continental shelf. "Memoires de la Societe Royale de Sciences de Liege, 6, 141-164.
Foster, N.M., Hudson, M.D., Bray, S. and Nicholls, R.J., 2013. Intertidal mudflat and saltmarsh conservation and sustainable use in the UK: A review. Journal of environmental management, 126, pp.96-104.
Francalanci, S., M. Bendoni, M. Rinaldi, and L. Solari (2013), Ecomorphodynamic evolution of salt marshes: Experimental observations of bank retreat processes, Geomorphology, 195(0), 53–65, doi:http://dx.doi.org/10.1016/j.geomorph.2013.04.026.
Haidvogel, D. B. et al. (2008), Ocean forecasting in terrain-following coordinates: Formulation and skill assessment of the Regional Ocean Modeling System, Journal of Computational Physics, 227(7), 3595–3624, doi:http://dx.doi.org/10.1016/j.jcp.2007.06.016.
Hall, T.M. and Sobel, A.H., 2013. On the impact angle of Hurricane Sandy's New Jersey landfall. Geophysical Research Letters, 40(10), pp.2312-2315.
Järvelä, J., 2002. Flow resistance of flexible and stiff vegetation: a flume study with natural plants. Journal of Hydrology, 269(1), pp.44-54.
Kennish, M. J. 2001, Physical Description of the Barnegat Bay—Little Egg Harbor Estuarine System, Journal of Coastal Research, 13–27, doi:10.2307/25736225.
Kirwan, M.L., Guntenspergen, G.R., D'Alpaos, A., Morris, J.T., Mudd, S.M. and Temmerman, S., 2010. Limits on the adaptability of coastal marshes to rising sea level. Geophysical Research Letters, 37(23).
Kirwan, M.L. and Megonigal, J.P., 2013. Tidal wetland stability in the face of human impacts and sea-level rise. Nature, 504(7478), pp.53-60.
Kirwan, M. and Temmerman, S., 2009. Coastal marsh response to historical and future sea-level acceleration. Quaternary Science Reviews, 28(17), pp.1801-1808.
Kirwan, M.L. and Murray, A.B., 2008. Ecological and morphological response of brackish tidal marshland to the next century of sea level rise: Westham Island, British Columbia. Global and Planetary Change, 60(3), pp.471-486.
Kirwan, M.L., Temmerman, S., Skeehan, E.E., Guntenspergen, G.R. and Fagherazzi, S., 2016. Overestimation of marsh vulnerability to sea level rise. Nature Climate Change, 6(3), pp.253-260.
Kumar, N., G. Voulgaris, and J. C. Warner (2011), Implementation and modification of a three-dimensional radiation stress formulation for surf zone and rip-current applications, Coastal Engineering, 58(12), 1097–1117, doi:http://dx.doi.org/10.1016/j.coastaleng.2011.06.009.
Koch, E. W. 1996. Hydrodynamics of a shallow Thalassia testudinum bed in Florida, USA. In Seagrass Biology – Proceedings of an International Workshop, Western Australia Museum, Perth, Australia. J. Kuo, R. C. Phillips, D. I. Walker and H. Kirkman, ed., 105-110
Lathrop Jr., R. G., and J. A. Bognar (2001), Habitat Loss and Alteration in the Barnegat Bay Region, Journal of Coastal Research, 212–228, doi:10.2307/25736235.
Lee, M., 2001. Coastal defence and the Habitats Directive: predictions of habitat change in England and Wales. The Geographical Journal 167 (1), 39-56.
Leonardi, N., and S. Fagherazzi (2014), How waves shape salt marshes, Geology , doi:10.1130/G35751.1.
Leonardi, N., and S. Fagherazzi (2015), Local variability in erosional resistance affects large scale morphodynamic response of salt marshes to wind waves, Geophysical Research Letters, 2015GL064730, doi:10.1002/2015GL064730.

© 2016 American Geophysical Union. All rights reserved.

Le Hir, P., Roberts, W., Cazaillet, O., Christie, M., Bassoullet, P. and Bacher, C., 2000. Characterization of intertidal flat hydrodynamics. Continental shelf research, 20(12), pp.1433-1459.
Limpert E, Stahel WA, Abbt M (2001) Log-normal Distributions across the Sciences: Keys and Clues: On the charms of statistics, and how mechanical models resembling gambling machines offer a link to a handy way to characterize log-normal distributions, which can provide deeper insight into v. BioScience 51 (5):341–352.
Malamud, B.D., 2004. Tails of natural hazards. Physics World, 17(8), p.25.
Marani, M., A. D'Alpaos, S. Lanzoni, and M. Santalucia (2011), Understanding and predicting wave erosion of marsh edges, Geophysical Research Letters, 38(21), L21401, doi:10.1029/2011GL048995.
Mariotti, G., Fagherazzi, S., Wiberg, P.L., McGlathery, K.J., Carniello, L. and Defina, A., 2010. Influence of storm surges and sea level on shallow tidal basin erosive processes. Journal of Geophysical Research: Oceans, 115(C11).
Mariotti, G. and Fagherazzi, S., 2013. Critical width of tidal flats triggers marsh collapse in the absence of sea-level rise. Proceedings of the national Academy of Sciences, 110(14), pp.5353-5356.
McLoughlin, S., P. Wiberg, I. Safak, and K. McGlathery (2015), Rates and Forcing of Marsh Edge Erosion in a Shallow Coastal Bay, Estuaries and Coasts, 38(2), 620–638, doi:10.1007/s12237-014-9841-2.
Möller, I., Spencer, T., French, J.R., Leggett, D.J. and Dixon, M., 1999. Wave transformation over salt marshes: a field and numerical modelling study from North Norfolk, England. Estuarine, Coastal and Shelf Science, 49(3), pp.411-426.
Möller, I., 2006. Quantifying saltmarsh vegetation and its effect on wave height dissipation: Results from a UK East coast saltmarsh. Estuarine, Coastal and Shelf Science, 69(3), pp.337-351.
Moller, I. et al. (2014), Wave attenuation over coastal salt marshes under storm surge conditions, Nature Geosci, 7(10), 727–731.
Mudd, S.M., Howell, S.M. and Morris, J.T., 2009. Impact of dynamic feedbacks between sedimentation, sea-level rise, and biomass production on near-surface marsh stratigraphy and carbon accumulation. Estuarine, Coastal and Shelf Science, 82(3), pp.377-389.
Murphy, A. H., and E. S. Epstein (1989), Skill Scores and Correlation Coefficients in Model Verification, Monthly Weather Review, 117(3), 572–582, doi:10.1175/1520-0493(1989)117<0572:SSACCI>2.0.CO;2.
Nepf, H.M., 1999. Drag, turbulence, and diffusion in flow through emergent vegetation. Water resources research, 35(2), pp.479-489.
NOAA NOS. 2012. National Ocean Service Hydrographic Survey data, National Oceanic and Atmospheric Administration, http://www. ngdc.noaa.gov/mgg/bathymetry/hydro.html. Accessed 2012.
Olabarrieta, M., Warner, J.C. and Kumar, N., 2011. Wave- current interaction in Willapa Bay. Journal of Geophysical Research: Oceans, 116(C12).
Orlanski, I., 1976: A simple boundary condition for unbounded hyperbolic flows. J. Comp. Sci., 21(3), 251-269.
Paramor, O.A.L. and Hughes, R.G., 2004. The effects of bioturbation and herbivory by the polychaete Nereis diversicolor on loss of saltmarsh in south- east England. Journal of Applied Ecology, 41(3), pp.449-463.
Pethick, J., 1993. Shoreline adjustments and coastal management: physical and biological processes under accelerated sea-level rise. Geographical Journal, pp.162-168.

© 2016 American Geophysical Union. All rights reserved.

Plater, A.J., Long, A.J., Spencer, C.D. and Delacour, R.A., 1999. The stratigraphic record of sea-level change and storms during the last 2000 years: Romney Marsh, southeast England. Quaternary International, 55(1), pp.17-27.
Psuty, N.P. and Ofiara, D.D., 2002. Coastal hazard management: Lessons and future directions from New Jersey. Rutgers University Press.
Prager, E. J., and R. B. Halley. 1999. The influence of seagrass on shell layers and FloridaBay mudbanks. Journal of Coastal Research 15:1151-1162.
Pye, K., French, P.W., 1993. Targets for Coastal Habitat Re-creation. Cambridge.
Ris, R. C., L. H. Holthuijsen, and N. Booij (1999), A third-generation wave model for coastal regions: 2. Verification, Journal of Geophysical Research: Oceans, 104(C4), 7667–7681, doi:10.1029/1998JC900123.
Schwimmer, R. A. (2001), Rates and Processes of Marsh Shoreline Erosion in Rehoboth Bay, Delaware, U.S.A., Journal of Coastal Research, 17(3), 672–683, doi:10.2307/4300218.
Shchepetkin, A. F., and J. C. McWilliams (2005), The regional oceanic modeling system (ROMS): a split-explicit, free-surface, topography-following-coordinate oceanic model, Ocean Modelling, 9(4), 347–404, doi:http://dx.doi.org/10.1016/j.ocemod.2004.08.002.
Schuerch, M., Vafeidis, A., Slawig, T. and Temmerman, S., 2013. Modeling the influence of changing storm patterns on the ability of a salt marsh to keep pace with sea level rise. Journal of Geophysical Research: Earth Surface, 118(1), pp.84-96.
Schuerch, M., Dolch, T., Reise, K. and Vafeidis, A.T., 2014. Unravelling interactions between salt marsh evolution and sedimentary processes in the Wadden Sea (southeastern North Sea). Progress in Physical Geography, 38(6), pp.691-715.
Suk, N.S., Guo, Q. and Psuty, N.P., 1999. Suspended solids flux between salt marsh and adjacent bay: a long-term continuous measurement. Estuarine, Coastal and shelf science, 49(1), pp.61-81.
Temmerman, S., Govers, G., Meire, P. and Wartel, S., 2003. Modelling long-term tidal marsh growth under changing tidal conditions and suspended sediment concentrations, Scheldt estuary, Belgium. Marine Geology, 193(1), pp.151-169.
Temmerman, S., Bouma, T.J., Govers, G., Wang, Z.B., De Vries, M.B. and Herman, P.M.J., 2005. Impact of vegetation on flow routing and sedimentation patterns: Three- dimensional modeling for a tidal marsh. Journal of Geophysical Research: Earth Surface, 110(F4).
Temmerman, S., P. Meire, T. J. Bouma, P. M. J. Herman, T. Ysebaert, and H. J. De Vriend (2013), Ecosystem-based coastal defence in the face of global change, Nature, 504(7478), 79–83.
Temmerman, S. and Kirwan, M.L., 2015. Building land with a rising sea. science, 349(6248), pp.588-589.
Tonelli, M., S. Fagherazzi, and M. Petti (2010), Modeling wave impact on salt marsh boundaries, Journal of Geophysical Research: Oceans, 115(C9), C09028, doi:10.1029/2009JC006026.
Tsujimoto, T., Kitamura, T., Fujii, Y., Nakagawa, H., 1996. Hydraulic resistance of flow with flexible vegetation in open channel. Journal of Hydroscience and Hydraulic Engineering 14 (1), 47–56.
UK National Ecosystem Assessment, 2011a. UK National Ecosystem Assessment: Chapter 11 Coastal Margins. UNEP/WCMC, Cambridge.
van de Koppel, J., van der Wal, D., Bakker, J.P. and Herman, P.M., (2005). Self-organization and vegetation collapse in salt marsh ecosystems. The American Naturalist, 165(1), pp.E1-E12.
van der Wal, D. and Pye, K., 2004. Patterns, rates and possible causes of saltmarsh erosion in the Greater Thames area (UK). Geomorphology, 61(3), pp.373-391.

© 2016 American Geophysical Union. All rights reserved.

Warner, J. C., C. R. Sherwood, R. P. Signell, C. K. Harris, and H. G. Arango (2008), Development of a three-dimensional, regional, coupled wave, current, and sediment-transport model, Computers & Geosciences, 34(10), 1284–1306, doi:http://dx.doi.org/10.1016/j.cageo.2008.02.012.

Warner, J. C., B. Armstrong, R. He, and J. B. Zambon (2010), Development of a Coupled Ocean–Atmosphere–Wave–Sediment Transport (COAWST) Modeling System, Ocean Modelling, 35(3), 230–244, doi:http://dx.doi.org/10.1016/j.ocemod.2010.07.010.

Zedler, J. B., and S. Kercher (2005), WETLAND RESOURCES: Status, Trends, Ecosystem Services, and Restorability, Annual Review of Environment and Resources, 30(1), 39–74, doi:10.1146/annurev.energy.30.050504.144248.

Zhao, H., and Q. Chen (2013), Modeling Attenuation of Storm Surge over Deformable Vegetation: Methodology and Verification, Journal of Engineering Mechanics, 140(12), 4014090, doi:10.1061/(ASCE)EM.1943-7889.0000704.

© 2016 American Geophysical Union. All rights reserved.

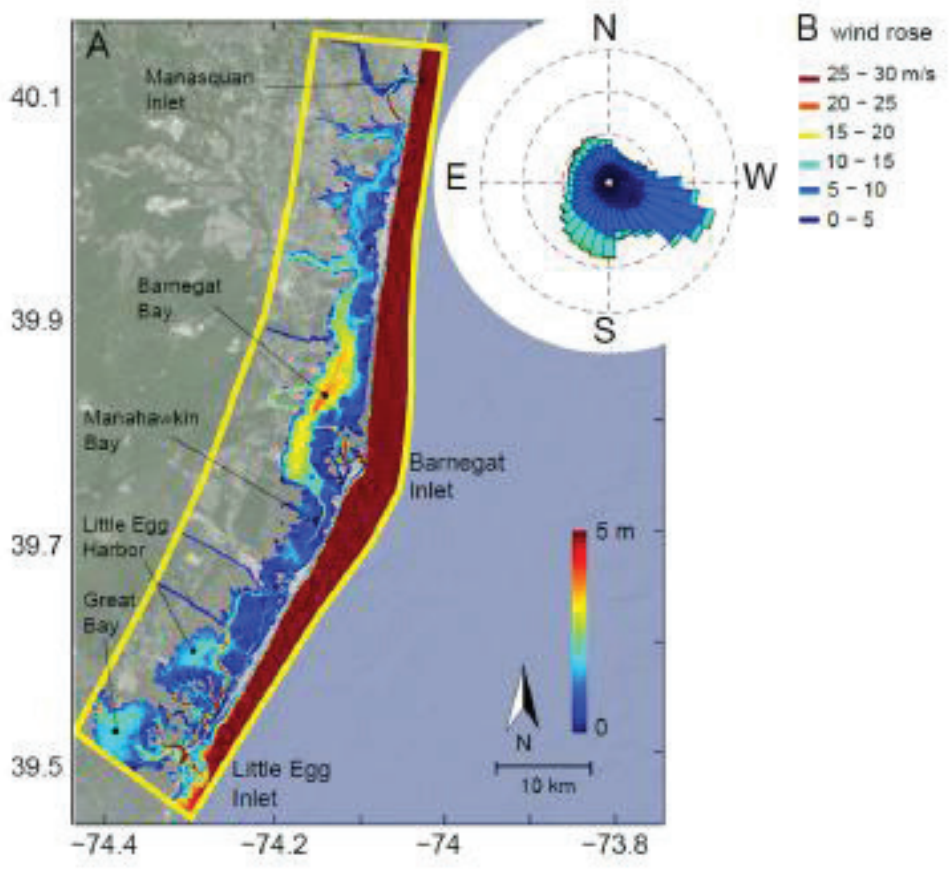

Figure 1 A) Bathymetry of the Barnegat Bay - Little Egg Harbor system. Yellow lines indicate the boundaries of the computational domain. B) Wind rose for the area for the period 1991-2013 (wind station, Station ID LLNR 830, 40°15'3" N 73°9'52" W).

© 2016 American Geophysical Union. All rights reserved.

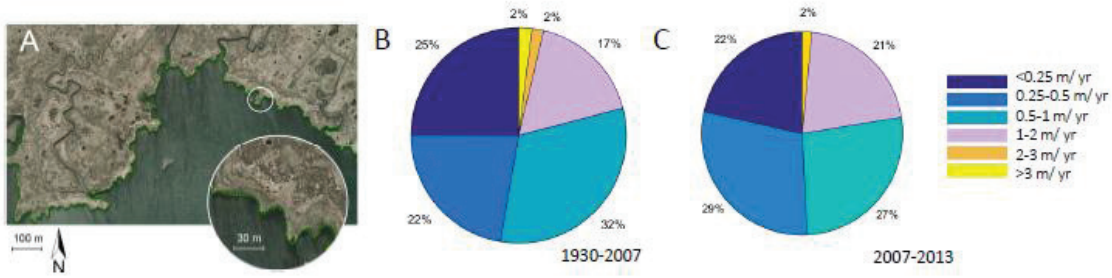

Figure 2 A) example of digitized shoreline (detail at lat. 39.64°, long. -74.22°). Fractions of total digitized shoreline subject to different erosion rates for the periods B) 1930-2007 and C) 2007-2013.

© 2016 American Geophysical Union. All rights reserved.

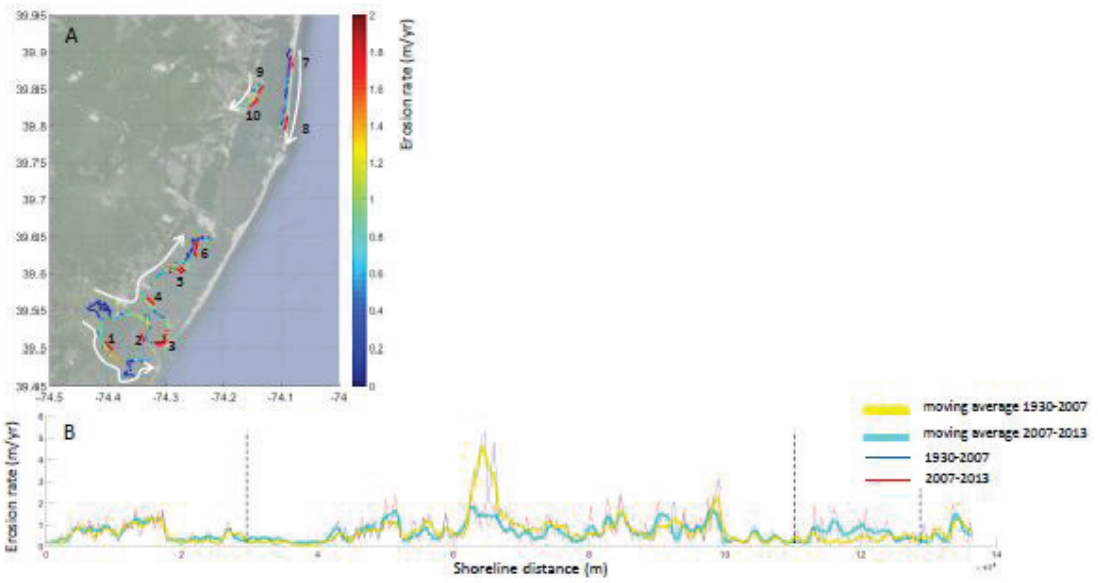

Figure 3 A) Spatial distribution of average erosion rates from 1930 to 2007. Numbers indicate portions of the shoreline that were also digitazed for the years 1995, 2002, and 2010. White arrows, as well as numbering order follow the alongshore coordinate plotted on the horizontal axis of panel B. B) Erosion rates as a function of the alongshore coordinate. Red and blue lines correspond to erosion rates for the periods 1930-2007 and 2007-2013 respectively. Yellow and cyan lines are moving averages of the same variables over a 1 km distance. The alongshore coordinate follows numbering in panel A. Vertical dashed lines separate portion of the alongshore coordinate covered by different arrows.

© 2016 American Geophysical Union. All rights reserved.

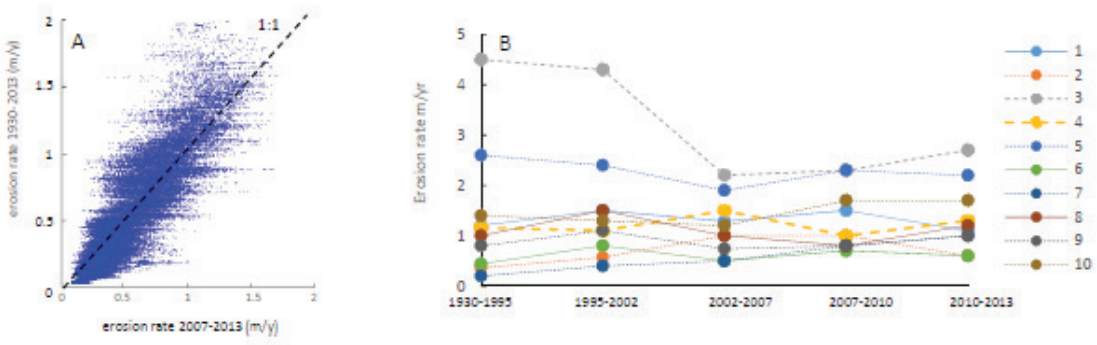

Figure 4 A) Comparison between average erosion rates from 2007 to 2013 and average erosion rates from 1930 to 2007 (R^2=0.76). B) Average erosion rate in different time intervals for ten stretches of shoreline having length of the order of 1 km, and whose locations are indicated in Figure 3A. Note that the period 2010-2013 includes hurricane Irene and hurricane Sandy.

© 2016 American Geophysical Union. All rights reserved.

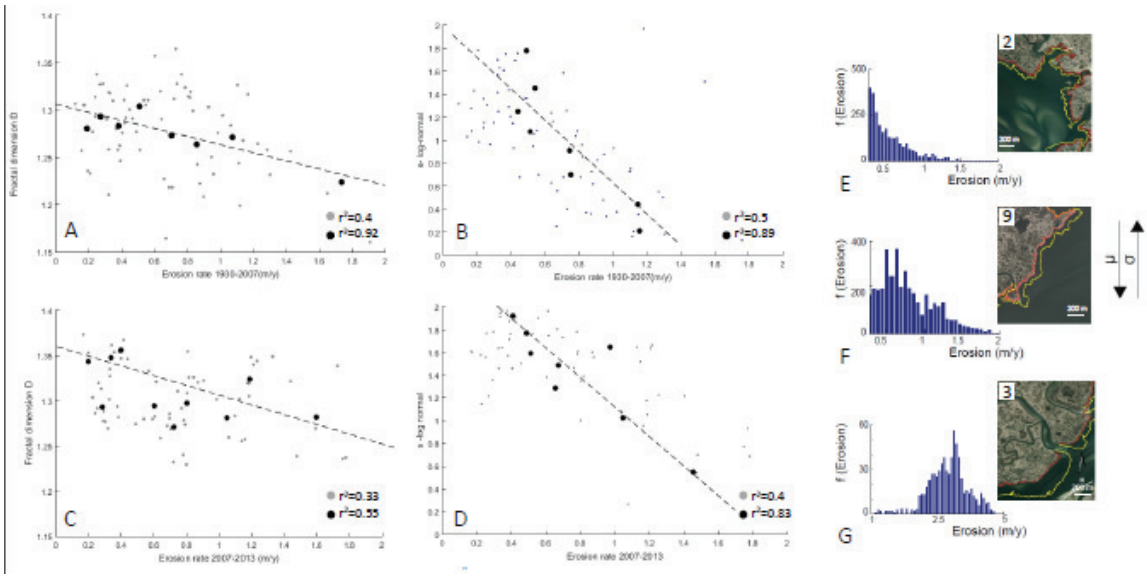

Figure 5 Relationship between erosion rate (horizontal axis), and fractal dimension (vertical axis) for the periods A) 1930-2007 and C) 2007-2013. Solid black circles indicate values obtained by averaging data over regular bins to emphasize the overall trend; Relationship between erosion rate (horizontal axis), and the log-normal standard deviation of the erosion events (vertical axis) for the periods B) 1930-2007 and D) 2007-2013. Solid black circles indicate values obtained by averaging data over regular bins to emphasize the overall trend; C, D, E examples of frequency magnitude distributions of erosion events for different stretches of shoreline, and corresponding shoreline images. For shoreline locations, see corresponding numbering in figure 2C.

© 2016 American Geophysical Union. All rights reserved.

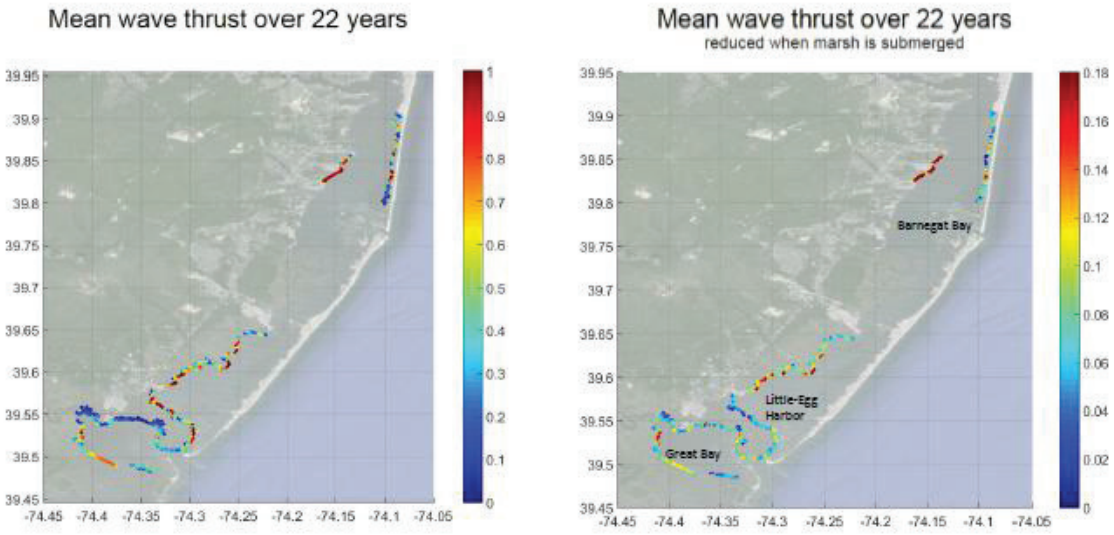

Figure 6 Map of average wave thrust values for the entire bay from 1991 to 2013.

© 2016 American Geophysical Union. All rights reserved.

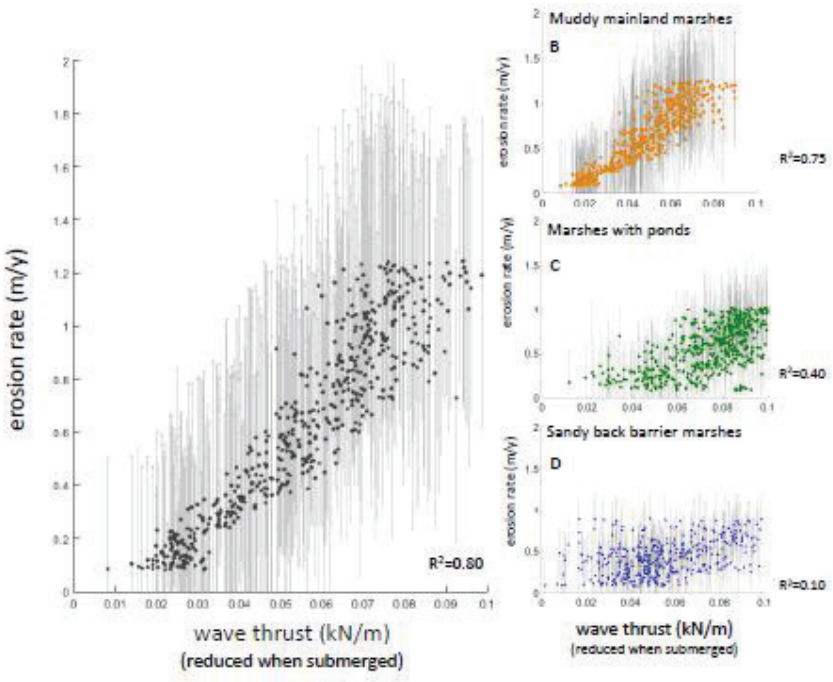

Figure 7 A) Relationship between erosion rate and wave thrust. Grey lines are error bars. A linear fit of gives linear coefficient of 11.915 m^2/kN/y. B),C) and D) Relationship between erosion rate and wave thrust for three different salt marsh categories corresponding to: mainland marshes, marshes with ponds, and back-barrier marshes. A linear fit of the points gives the following coefficients: 14.32, 8.30, and 7.11 m^2/kN/y respectively.

© 2016 American Geophysical Union. All rights reserved.

Journal of Geophysical Research: Earth Surface

Supporting Information for

Salt marsh erosion rates and boundary features in Barnegat Bay, New Jersey, USA

Nicoletta Leonardi[1,3], Zafer Defne[2], Neil K. Ganju[2], Sergio Fagherazzi[3]

[1]Department of Geography and Planning, University of Liverpool, UK

[2]United States Geological Survey, Woods Hole MA, USA

[3]Department of Earth and Environment, Boston University, Boston , MA, USA

Contents of this file

Methods: Wave thrust subroutine

Results: (Figure S1) Hurricanes tracks interesting New Jersey from 2007 to 2013; Images of before and after Hurricane Sandy.

Introduction

We provide the code necessary to run the offline wave thrust calculations presented in the paper. The same code has been implemented into the COWAST modeling suite (http://woodshole.er.usgs.gov/operations/modeling/COAWST/).

We further provide information relevant to the occurrence of Hurricane in the area for the period in between 2007, and 2013 (Figure S1).

```
function [EFstar,WFstar,EF_TOT,WF_TOT,bou_wd_nan,bou_wd_msl_nan,
bou_wd_msl_nan2,lat_rho,lon_rho,thrust_w_noangle,...
thrust_w,thrust_w_msl,thrust_w_wet,thrust_w_noangle_msl,thrust_w_noangle_wet,mask_wd_tonelli,thrust_w_t
onelli,Pwave2,Hwave2] =...
risk (flag_mask_msl,start,nt,T_hours,grid_type,taucr,Pcr,percent,name_history_file,name_swan_file);
% LAST UPDATE = Fabruary 2_April2015
% EVALUATE MARSH THRUST, WAVE FACTOR AND EROSION FACTOR AT MARSH BOUNDARIES
% [For Erosion and Wave Factors see:
% Fagherazzi and Wiberg, 2009; Mariotti and Fagherazzi,
% 2010 "Influence of storm surges and sea level on shallow tidal basin
% erosive processes" (euqation 15 and 17);
% For wave Thrust see: Tonelli et al;, 2010
% "Modeling wave impact on salt marsh boundaries"].
% For wave thrust see also: "water waves mechanics for engineers and
% scientists" by Dean and Darlymple].
% Marsh thrust values are calculated with and without the correction from
% wave angle.
% For each cell if one side of the cell is sheletred from other
% cells, that side is not exposed to waves.
% Each cell has four normals directed towards the center of the cell.
% the angle of the normals is respect to the north and clockwise.
% You can apply the Tonelli mask to reduce the value of the wave thrust
% when marsh is submerged
%
% --------------------------------INPUT-----------------------------------
% 1) name_hystory_file = is the name of the ROMS history file. Insert it
% using ''. e.g [...]=risk ('ocean_his.nc','swan_ocean.nc',....
% 2) name_swan_file = is the name of the SWAN output file or roms input
% file if SWAN was runned in another simulation like in shoreface test case
%
% 3) flag_mask_msl==1 it means you want contour at mean sea level
% flag_mask_msl==0 it means you don't want contour at mean sea level
%
% 4)start= initial time step to do the anlysis
% 5)nt= number of time steps for the analysis
% 6) T_hours time during which you want to average the Erosion factor and
% the wave factor
% 7) grid_type; if equal to 1 it means that have latitude and longitude
% If equal to 0 it means I only have x and y
% 8) taucr, the critical shear stress for the marsh boundary
% 9) Pcr, the critical wave power marsh boundary
% 10) percent is the percentage of time to be inundated to be considered
% tidal flat. For example, In shoreface the wet dry mask is at the
% longitudinal grid point 45 for 101 time steps (for 120 total time step)
% While it is at the longitudianl grid point 44 for 20 time step. If
% percent=0. Points at longitudinal coordiante 44 are tidal flat. If
% percent=21 points at longitudinal coordiante 44 are NOT tidal flat.
% --------------------------------OUTPUT----------------------------------
% Asterisks mean that they are the main outputs.
%
% --EFstar is the erosion factor for each point of the boundary for each time
% step (EFstar=Area_cell.*(bstr-bucr))
%
% --WFstar is the wave factor for each point of the boundary for each time
% step (WFstar=Pwave.*length exposed site)
%
% **--EF_TOT is the erosion factor of the entire boundary averaged over a
% period of T_hours (T_hours defined in the input)
%
% **--WF_TOT is the wave factor of the entire boundary averaged over a
% period of T_hours (T_hours defined in the input)
%
% --bou_wd_nan is the wet contour for each time step. points equal to one
% are the last wet points
%
% --bou_wd_msl_nan is the wet contour at mean sea level. Is the contour for
% which the marsh thrust is evaluated with the tonelli
%
% --bou_wd_msl_nan2 is the wet contour and it is thick three cell instead
% fo one cell.
%
% --thrust_w is the map of the marsh thrust for the entire domain. you need
% to multiply this for the wet contour or for the contour at mean sea level,
% or for the contour which is three cell thick to have the thrust on the
% marsh. The results will be thrust_w_msl or thrust_w_wet.
%
```

```
% **--thrust_w_msl thrust along the contour at mean sea level for each time step.
% This imply that marshes elevation are at mean sea level. You can apply
% the tonelli mask to obtain the thrust reduction. This take into accout
% wave direction.
%
% **--thrust_w_wet thrust along the wet contour for each time step. The wet
% contour change with the time step and depends on the water level.
% You CAN NOT apply the Tonelli mask to this because Tonelli mask make
% sense if the contour is fixed in time and interested by different water
% level depths. This take into accoutn wave direction
%
% --thrust_w_noangle_msl thrust at msl without the angle correction
%
% --thrust_w_noangle_wet thrust wet contour without angle correction
%
% **--thrust_w_tonelli wave thrust along mean sea level with marsh thrust
% reduction in case of salt marsh submergence
%
% **--mask_wd_tonelli mask to apply to thrust_w_msl to obtain thrust_w_tonelli
%
% start=100;
% nt=10;
% T_hours=3;
% grid_type=1;
% taucr=0;
% Pcr=0;
% percent=0;
% flag_mask_msl=1;
%
name_history_file='http://geoport.whoi.edu/thredds/dodsC/clay/usgs/users/abeudin/chinco/tidewindwave/hi
s_v3.nc';
% name_history_file='last.nc';
%
% [EFstar,WFstar,EF_TOT,WF_TOT,bou_wd_nan,bou_wd_msl_nan,
bou_wd_msl_nan2,lat_rho,lon_rho,thrust_w_noangle,...
%
thrust_w,thrust_w_msl,thrust_w_wet,thrust_w_noangle_msl,thrust_w_noangle_wet,mask_wd_tonelli,thrust_w_t
onelli] =...
% risk (flag_mask_msl,start,nt,T_hours,grid_type,taucr,Pcr,percent,name_history_file);
%
% %-------------------------------------------------------------------------
% %-------------------------------------------------------------------------
% %-------------------------------------------------------------------------
% % EXPORT DATA FROM HISTORY FILE
% %-------------------------------------------------------------------------
warning off;
g=9.81;
T=T_hours.*60.*60;
nc=ncgeodataset(name_history_file);
hc=(nc{'hc'}(:));
t=(nc{'ocean_time'}(:)); % Time vector
dt =(t(2)-t(1)); % dt_hour = time inetrval between following hystory record
dt_hour = dt./60./60;
nn=round((T./dt)-1); % nn=number of interval to average
n_T=t(1:nn:end)'; % t evaluated at the boundary between subsequent time intervals
ntav=length(n_T); % number of intervals
if grid_type==0;
x_rho=squeeze(nc{'x_rho'});
number_cell=size(x_rho);
nx=number_cell(1); % nx = number of x_rho points
ny=number_cell(2); % ny = number of y_rho points
else
lon_rho=squeeze(nc{'lon_rho'}(:));
number_cell=size(lon_rho);
nx=number_cell(1); % nx = number of x_rho points
ny=number_cell(2); % ny = number of y_rho points
end
% %-------------------------------------------------------------------------
% % FIND THE WET-DRY BOUNDARY AT MEAN SEA LEVEL
% % (assume that marshes elevation is at mean sea level)
% %-------------------------------------------------------------------------
if flag_mask_msl==1
dt24=floor(12.*60.*60./dt); % number of time step to reach the first 24 hours
if nt>dt24; % If you are analyzing more than 24 hours use this to find the boundary
at msl
[bou_wd_msl,bou_wd_msl_nan,bou_wd_msl_nan2]=contour_msl(nc,dt24,nx,ny);
```

```
else % if you have less than 24 hours you cannot evaluate the boundary at
mean sea level
bou_wd_msl=nan; % give nan value because you cannot calculate them becuase you don't
have entire tidal cycle.
bou_wd_msl_nan=nan; % give nan value because you cannot calculate them
bou_wd_msl_nan2=nan; % give nan value because you cannot calculate them
end
else
bou_wd_msl=nan; % give nan value because the user don't want it
bou_wd_msl_nan=nan; % give nan value because the user don't want it
bou_wd_msl_nan2=nan; % give nan value because the user don't want it
end
% %--------------------------------------------------------------------------
% % INITIALIZE VARIABLES
% %--------------------------------------------------------------------------
thrust_w_msl=nan(nt,nx,ny); % initialize Marsh Thrust for the boundary at mean sea level
thrust_w_msl_tonelli=nan(nt,nx,ny); % initialize Marsh Thrust for the boundary at mean sea level
TONELLI(=REDUCTION WHEN CREST HIGHER THAN MARSH)
thrust_w=nan(nt,nx,ny); % initialize Marsh Thrust
bou_wd=zeros(nt,nx,ny); % Initialize the wet-dry boundary
mask_wd_tonelli=zeros(nt,nx,ny); % Mask Tonelli (to apply if I want to reduce the thrust when th marsh
is
submerged)
EFstar=zeros(nt,nx,ny); % Initialize shear stress factor every time step
WFstar=zeros(nt,nx,ny); % Initialize wave factor every time step
EF=zeros(ntav,nx,ny); % Initialize shear stress factor averaged every nn time steps
EF_TOT=zeros(ntav,1);
WF=zeros(ntav,nx,ny); % Initialize wave factor averaged every nn time steps
Atf=zeros(ntav,1);
bucr=taucr.*ones(nx,ny); % Initialize critical value of shear stress in the domain
dir_r=zeros(nx,ny); % Initialize direction of the right side of the cells
dir_l=zeros(nx,ny); % Initialize direction of the left side of the cells
dir_b=zeros(nx,ny); % Initialize direction of the bottom side of the cells
dir_u=zeros(nx,ny); % Initialize direction of the upper side of the cells
bou_wd_r=zeros(nx,ny); % Initialize areas of the wet-dry boundary with left neighbours (these
are used in the "find neighbours section)
bou_wd_l=zeros(nx,ny); % Initialize areas of the wet-dry boundary with right neighbours (these
are used in the "find neighbours section)
bou_wd_b=zeros(nx,ny); % Initialize areas of the wet-dry boundary with upper neighbours (these
are used in the "find neighbours section)
bou_wd_up=zeros(nx,ny); % Initialize areas of the wet-dry boundary with bottom neighbours (these
are used in the "find neighbours section)
gg=0; % Index for erosion and wave factor
% %--------------------------------------------------------------------------
% % DOWNLOAD THE DATA FROM NETCDF FILES
% %--------------------------------------------------------------------------
for n_t=1:nt;
ff=start+n_t;
if nargin>9 % The user input both a ocean histroy file and a swan file
[lat_rho,lat_u,lat_v,lon_rho,lon_u,lon_v,x_rho,y_rho,...
x_u,y_u,x_v,y_v,z,mask_wd,mask_wd_u,mask_wd_v,bustr_rho,bvstr_rho,Hwave,Pwave_top,Pwave_bot,Lwave,Dwave
,ndims_h,h,ro0]...
= download(grid_type,ff,name_history_file,name_swan_file);
else % The user only input a ocean histroy file and a swan file
[lat_rho,lat_u,lat_v,lon_rho,lon_u,lon_v,x_rho,y_rho,...
x_u,y_u,x_v,y_v,z,mask_wd,mask_wd_u,mask_wd_v,bustr_rho,bvstr_rho,Hwave,Pwave_top,Pwave_bot,Lwave,Dwave
,ndims_h,h,ro0]...
= download(grid_type,ff,name_history_file);
end
ff=n_t;
% %--------------------------------------------------------------------------
% % ALL DATA USED BELOW NEED TO BE DOWNLOADED BEFORE WITH THE THER SCRIPT
% %--------------------------------------------------------------------------
% % PRELIMINARY OPERATIONS WITH DATA
% %--------------------------------------------------------------------------
size_rho=size(x_rho); % Number of rho points
size_u=size(x_u); % Number of u points (note x_u has same dimension than y_u)
size_v=size(x_v); % Number of v points (note x_v has same diemanion than y_v)
x_rho_t(:,:)=x_rho; % rho points
y_rho_t(:,:)=y_rho;
lon_rho_t(:,:)=lon_rho;
lat_rho_t(:,:)=lat_rho;
lon_u_t(:,:)=lon_u;
lat_u_t(:,:)=lat_u;
lon_v_t(:,:)=lon_v;
lat_v_t(:,:)=lat_v;
```

```
depth_all=z+h; % Depth for each ocean time, for every rho point
depth=depth_all.*mask_wd; % Depth for each ocean time, only wet cells
l_x=abs([2*(x_u(:,1)-x_rho(:,1)),...
x_u(:,2:end)-x_u(:,1:end-1),... % Cells width along x axis. Centers are the rho points
2*(x_rho(:,end)-x_u(:,end))]); % For the boundary points the width is found considerin the half cell
going from rho to u.
l_y=abs([2*(y_v(1,:)-y_rho(1,:));... % Cells width along y axis. Centers are the rho points
y_v(2:end,:)-y_v(1:end-1,:);... % For the boundary points the width is found considerin the half cell
going from rho to u.
2*(y_rho(end,:)-y_v(end,:))]);
% %-------------------------------------------------------------------------
% % FIND THE WET POINTS OF BOUNDARIES AND TIDAL FLAT
% %-------------------------------------------------------------------------
% % method:
% 1 1 1 0 0 0 -
% 1 1 1 0 0 0
% _____________________________
% 0 0 1 0
%
% % THIS BOUNDARY IS DEFINED AT THE RHO POINTS:For this use the u and v
% % coordinate to find it.
% % The position of 1 is the last dry point (try plot mask_wd_u and
% % bou_wd_u1 for exmaple. I do this operation back and forth (using
% % bou_wd_u1/ bou_wd_u2 and summing them together.
% % I do the same for
% % bou_wd_v1/bou_wd_v2 using the mask_wd_v . I do it with the mask_wd_u and
% % mask_wd_v To get all the boundary points that I would not get because
% % mask_wd_u and mask_wd_v have differetn size than mask_wd_rho.
%%
% %-------------------------------------------------------------------------
% CALCULATE BOUNDARY (APRIL 8 2015)
%-------------------------------------------------------------------------
% This is for the vertical direction
%-------------------------------------------------------------------------
bou_wd1=zeros(nt,nx,ny);
bou_wd1(ff,1:nx-1,:)=(mask_wd(1:end-1,:)... % boundary wet and dry. Points equl to 1 are last wet
point; points
equalt to -1 are last dry point
-mask_wd(2:end,:));
bou_wd1((bou_wd1==-1))=0; % I exclude from the result the dry points because I only want the wet
ones
% bou_wd1((bou_wd1~=0))=1;% should not be necessary but retry
% Now I do the other direction because I don't know if it is 000111 or
% 111000
bou_wd2=zeros(nt,nx,ny);
bou_wd2(ff,2:nx,:)=(mask_wd(2:end,:)... % boundary wet and dry. Points equl to 1 are last wet point;
points
equalt to -1 are last dry point
-mask_wd(1:end-1,:));
bou_wd2((bou_wd2==-1))=0;
bou_wd2((bou_wd2~=0))=1;
bou_wdv=bou_wd1+bou_wd2;
bou_wdv(bou_wdv==-1)=0;
% bou_wdv(bou_wd~=0)=1;%should not be necessary but retry
% close all % do plot to test whta it did
% pcolor(squeeze(bou_wdv(ff,1:10,1:10)));
% figure
% pcolor(squeeze(mask_wd(1:10,1:10)));
%-------------------------------------------------------------------------
% This is for the horizontal direction
%-------------------------------------------------------------------------
bou_wd1=zeros(nt,nx,ny);
bou_wd1(ff,:,1:ny-1)=(mask_wd(:,1:end-1)... % boundary wet and dry. Points equl to 1 are last wet
point; points
equalt to -1 are last dry point
-mask_wd(:,2:end));
bou_wd1((bou_wd1==-1))=0; % I exclude from the result the dry points because I only want the wet
ones
% bou_wd1((bou_wd1~=0))=1; %should not be necessary but retry
% Now I do the other direction because I don't know if it is 000111 or
% 111000
bou_wd2=zeros(nt,nx,ny);
bou_wd2(ff,:,2:ny)=(mask_wd(:,2:end)... % boundary wet and dry. Points equl to 1 are last wet point;
points
equalt to -1 are last dry point
-mask_wd(:,1:end-1));
```

```
bou_wd2((bou_wd2==-1))=0;
bou_wd2((bou_wd2~=0))=1;
bou_wdh=bou_wd1+bou_wd2;
bou_wdh(bou_wdh==-1)=0;
% bou_wdh(bou_wd~=0)=1;%should not be necessary but retry
% close all % plot to see waht it did
% pcolor(squeeze(bou_wdh(ff,1:10,1:10)));
% figure
% pcolor(squeeze(mask_wd(1:10,1:10)));
%--------------------------------------------------------------------------
% calculate bou_wd_nan
%--------------------------------------------------------------------------
bou_wd=bou_wdv+bou_wdh;
bou_wd(bou_wd~=0)=1;
bou_wd_nan=bou_wd;
bou_wd_nan(bou_wd==0)=nan;
% % THIS IS THE TEST. TO work it should be all2
% test2=squeeze(bou_wd_nan(ff,:,:))+mask_wd;
% pcolor((test2));shading flat
% %--------------------------------------------------------------------------
% %--------------------------------------------------------------------------
% % FIND ANGLE
% %--------------------------------------------------------------------------
% % Find the angle respect to cartesian cordiante system.
% % Angles are measured clockwise from the north. Zero means North. 270
% % means west.
% % Find orthogonal direction to the 4 sides of each rho_point (i.e the
% % orthogonals are lines connecting different rho points)
% % |
% % x___v____x
% % -->| rho- |<-- rho
% % |x_______x|
% % ^
% % |
% % The angles of the orthogonal refer TO THE NORTH CLOCKWISE DIRECTION
% % the normal as the head toward the surface like in the sketch.
% % The angle is the angle orthogonal to the four sides. It differs from
% % the variable angle which is an average at the rho points.
% % I associate to each rho point 4 directions. For the boundary rho points
% % one of the directions is missed (because the grid ends and there are
% % not other rho points on one of the sides. So I associated to it a nan
% %--------------------------------------------------------------------------
% %--------------------------------------------------------------------------
if grid_type==1
dir_b(2:end-1,:)=dir_cell(lat_rho_t(2:end-1,:),lat_rho_t(1:end-2,:),...
lon_rho_t(2:end-1,:),lon_rho_t(1:end-2,:)); % Direction orthogonal bottom side rho point, using
Adjacent rho points
dir_u(2:end-1,:)=dir_cell(lat_rho_t(2:end-1,:),lat_rho_t(3:end,:),...
lon_rho_t(2:end-1,:),lon_rho_t(3:end,:)); % Direction orthogonal upper side rho point, using Adjacent
rho points
dir_l(:,2:end-1)=dir_cell(lat_rho_t(:,2:end-1),lat_rho_t(:,1:end-2),...
lon_rho_t(:,2:end-1),lon_rho_t(:,1:end-2)); % Direction orthogonal left side rho point, using Adjacent
rho points
dir_r(:,2:end-1)=dir_cell(lat_rho_t(:,2:end-1),lat_rho_t(:,3:end),...
lon_rho_t(:,2:end-1),lon_rho_t(:,3:end)); % Direction orthogonal right side rho point, using Adjacent
rho points
dir_r(:,1)=-dir_l(:,2); % It is equal to the opposite direction of the subsequent point. But the
normal point opposite so I adds ign minus
dir_r(:,end)=nan; % It does not exist because there are not rho points after it
dir_l(:,1)=nan; % It does not exist because therea are not rho points before it
dir_l(:,end)=-dir_r(:,end-1);
dir_u(1,:)=-dir_b(2,:);
dir_u(end,:)=nan;
dir_b(1,:)=nan; % It does not exist becasue there is not another rho points on the left
side
dir_b(end,:)=-dir_u(end-1,:);
else %lat is y and lon is x
dir_b(2:end-1,:)=dir_cell(y_rho_t(2:end-1,:),y_rho_t(1:end-2,:),...
x_rho_t(2:end-1,:),x_rho_t(1:end-2,:)); % Direction orthogonal bottom side rho point, using Adjacent
rho points
dir_u(2:end-1,:)=dir_cell(y_rho_t(2:end-1,:),y_rho_t(3:end,:),...
x_rho_t(2:end-1,:),x_rho_t(3:end,:)); % Direction orthogonal upper side rho point, using Adjacent rho
points
dir_l(:,2:end-1)=dir_cell(y_rho_t(:,2:end-1),y_rho_t(:,1:end-2),...
x_rho_t(:,2:end-1),x_rho_t(:,1:end-2)); % Direction orthogonal left side rho point, using Adjacent rho
points
```

```
dir_r(:,2:end-1)=dir_cell(y_rho_t(:,2:end-1),y_rho_t(:,3:end),...
x_rho_t(:,2:end-1),x_rho_t(:,3:end)); % Direction orthogonal right side rho point, using Adjacent rho
points
dir_r(:,1)=-dir_l(:,2); % It is equal to the opposite direction of the subsequent point. But the
normal point opposite so I adds ign minus
dir_r(:,end)=nan; % It does not exist because there are not rho points after it
dir_l(:,1)=nan; % It does not exist because therea are not rho points before it
dir_l(:,end)=-dir_r(:,end-1);
dir_u(1,:)=-dir_b(2,:);
dir_u(end,:)=nan;
dir_b(1,:)=nan; % It does not exist becasue there is not another rho points on the left
side
dir_b(end,:)=-dir_u(end-1,:);
end
% %-------------------------------------------------------------------------
% % FIND NEIGHBOURS
% %-------------------------------------------------------------------------
% % To find the neighbours:
% % Method: I have 4 possible directions from one boundary cell to the
% % others. For the boundary points equal to 1 are wet;
% % While points equal to 0 are dry.
% % I slide the wet dry mask on the right and I sum with the original mask.
% % I can the following results for each cell:
% % 2=the cell is wet and I have a wet neighbour on the left;
% % 1= the cell is dry and I have a wet neighbour on the left;
% % 1=The cell is wet and I have a dry neighbour on the left
% % For all the cases where I have a result equal to 1 I cannot
% % calculate the trhust at that point for a given direction either because
% % the point is dry (and It would be deleted in any case with the boundary
% % contour) or because the point is sheltered from that given direction.
% % Example:
% % Original matrix
% % ___|____|____|____|_____
% % ___|__1_|____|____|_____
% % ___|__1_|__1_|____|_____
% % ___|____|____|__1_|___1_
% % | | | |
% % I add to the original the following matrix (slided to the rigth)
% % ___|____|____|____|____|
% % ___|____|__1_|____|____|
% % ___|____|__1_|__1_|____|
% % ___|____|____|____|__1_|
% % | | | |
% % And I obtain:
% % ___|____|____|____|_____
% % ___|__1_|__1_|____|_____
% % ___|__1_|__2_|____|_____
% % ___|____|____|__1_|___2_
% % | | | |
% % I repeat the same operation for the four directions
% %-------------------------------------------------------------------------
% % An isolated cell can be: 1)a water cell with four dry neighbours or 2)
% % dry cell with 4 wet neighbours. in the second cell it is going to be
% % set to zero when multipliying fot eh wet contour.
% %-------------------------------------------------------------------------
% %-------------------------------------------------------------------------
Isolated_cell_l=zeros(nx,ny); % Initialize possible isolated water cell found sliding to the right
Isolated_cell_r=zeros(nx,ny); % Initialize possible isolated water cell found sliding to the left
Isolated_cell_up=zeros(nx,ny); % Initialize possible isolated water cell found sliding to the bottom
Isolated_cell_b=zeros(nx,ny); % Initialize possible isolated water cell found sliding up
bou_wd_l(:,2:end)=mask_wd(:,1:end-1); % Find neighbours on th right
sum_l=((mask_wd(:,:))+bou_wd_l); % Sum of original matrix and matrix slided to the right. The result
can
only be 1 or 2;
l_star=find(sum_l~=2); % if the sum is two it means it is a wet cell with a wet neighbour which
can be attacked by waves
Isolated_cell_l(l_star)=1; % Set to 1 the cells which could be Isolated
sum_l(l_star)=nan; % Set to nan values which CANNOT be attacked either becuase tehy are dry
cell or because they are sheltered
sum_l(sum_l==2)=1; % Set to 1 values which can be attacked
% Find neighbours on the left
bou_wd_r(:,1:end-1)=mask_wd(:,2:end);
sum_r=(mask_wd(:,:)+bou_wd_r);
r_star=find(sum_r~=2);
Isolated_cell_r(r_star)=1;
sum_r(r_star)=nan;
```

```
sum_r(sum_r==2)=1;
% Find neighbours at the bottom
bou_wd_up(2:end,:)=mask_wd(1:end-1,:);
sum_u=(mask_wd(:,:)+bou_wd_up);
u_star=find(sum_u~=2);
Isolated_cell_up(u_star)=1;
sum_u(u_star)=nan;
sum_u(sum_u==2)=1;
% Find neighburs at the top
bou_wd_b(1:end-1,:)=mask_wd(2:end,:);
sum_b=(mask_wd(:,:)+bou_wd_b);
b_star=find(sum_b~=2);
Isolated_cell_b(b_star)=1;
sum_b(b_star)=nan;
sum_b(sum_b==2)=1;
% Find the Isolated cell
Isolated_cell=Isolated_cell_r+Isolated_cell_l+...
Isolated_cell_b+Isolated_cell_up;
Isolated_cell(Isolated_cell~=4)=nan; % This is a necessary (not sufficient0 condition to be an isolated
cell
Isolated_cell(Isolated_cell==4)=1; % I set possible isolated cell equl to 1
Isolated_cell=Isolated_cell+mask_wd;
Isolated_cell(Isolated_cell~=2)=0; % Where this sum is zero it means that the cell is both Isolated and
wet
Isolated_cell(Isolated_cell==2)=1;
toadd_isolated=find(Isolated_cell(:,:)==1); % Points where thrust need to be evaluated because they are
isolated
cells
bou_wd(ff,toadd_isolated)=1; % Add isolated points to the boundary points
sum_r(toadd_isolated)=1; % Add isolated points to the wet right neighbours
sum_l(toadd_isolated)=1; % Add isolated points to the wet left neighbours
sum_u(toadd_isolated)=1; % Add isolated points to the wet up neighbours
sum_b(toadd_isolated)=1; % Add isolated points tothe wet bottom neighbours
% Note: sum_r,_l,_u,_b have values 1 or 0; dir_r,...is the angle in deg
exp_r=dir_r.*sum_r.*squeeze(bou_wd(ff,:,:)); % Only maintain the direction of the RIGHT sides of the
rho points where
there ae NOT neighbours
exp_l=dir_l.*sum_l.*squeeze(bou_wd(ff,:,:)); % Only maintain the direction of the LEFT sides of the rho
points where
there are NOT neighbours
exp_u=dir_u.*sum_u.*squeeze(bou_wd(ff,:,:)); % Only maintain the direction of the UPPER sides of the
rho points where
there are NOT neighbours
exp_b=dir_b.*sum_b.*squeeze(bou_wd(ff,:,:)); % Only maintain the direction of the BOTTOM sides of the
rho points
where there are NOT neighbours
% %-------------------------------------------------------------------------
% % CALCULATE THE MARSH THRUST
% %-------------------------------------------------------------------------
% % also see water waves mechanics for engineering and scientists
% % Dean Darlymple, pg 84 for formula. pg 77 for sketch of the variables.
% % Thrust=inetgral in z of the dynamic pressure;
% % Dynamic pressure = ro.*g.*max(z_thrust).*Kp(z_thrust);
% %
% % Kp=pressure response factor:
% % Kp(z_thrust)=(cosh(kw.*(h+z_thrust))./(cosh(kw.*h))
% %
% % The integral of the pressure response factor in z_thrust:
% % Integral_Kp=sinh(kw*(h + z_thrust))/(kw*cosh(h*kw))
% %
% % z_thrust is the vertical coordinate going from -h to + z
% %(roms variable). z_thrust is thus 0 at msl, positive above msl and
% % negative below msl. below I directly use the expression of the integral
% %-------------------------------------------------------------------------
% %-------------------------------------------------------------------------
% % THRUST WITH ANGLE CORRECTION
% % (270 deg)--> ------- <--(90 deg)
% % ^
% % |
% % (0 deg)
% % If the absolute value of the difference between wave direction and
% % normal directed inside the cell is between 90 and 270 deg it means that
% % the flow is blowing opposite direction
% %-------------------------------------------------------------------------
kw=2*pi./Lwave; % wave number
```

```
Integral_Kp=sinh(kw.*(h+0))./(kw.*cosh(h.*kw)); % Integral of Pressure response factor at msl; above
msl I use
hydostatic approximation and I don't need Kp
% F_pd_h=sinh(kw.*(h-h))./(kw.*cosh(h.*kw)); % This is always zero
Fw1=ro0.*9.81.*Hwave.*Integral_Kp./1000; % Dynamic pressure below m.s.l (divide 1000 to have KN); roms
variable z is max(z_thrust)
Fw2=(ro0*9.81.*Hwave).*Hwave./2./1000; % Idrostatic approximation above m.s.l (divide 1000 to have KN);
Fw=Fw1+Fw2; % Total Wave thrust above mean sea lveel
thrust_r=abs(Fw.*cosd(exp_r-Dwave));
thrust_r(abs(exp_r-Dwave)>=90 & abs(exp_r-Dwave)<=270)=0; % If the angle is higher than 90 and smaller
than 270 it means that that
waves are
thrust_r(isnan(thrust_r))=0; % arriving opposite direction respect to the cell side(impact other
side, e.g impact right
% and not the left side of the cell.
thrust_l=abs(Fw.*cosd(exp_l-Dwave));
thrust_l(abs(exp_l-Dwave)>=90 & abs(exp_l-Dwave)<=270)=0;
thrust_l(isnan(thrust_l))=0;
thrust_b=abs(Fw.*cosd(exp_b-Dwave));
thrust_b(abs(exp_b-Dwave)>=90 & abs(exp_b-Dwave)<=270)=0;
thrust_b(isnan(thrust_b))=0;
thrust_u=abs(Fw.*cosd(exp_u-Dwave));
thrust_u(abs(exp_u-Dwave)>=90 & abs(exp_u-Dwave)<=270)=0;
thrust_u(isnan(thrust_u))=0;
% %-------------------------------------------------------------------------
% % THRUST WITH NO ANGLE CORRECTION
% %-------------------------------------------------------------------------
thrust_r_noangle=Fw.*sum_r;
thrust_r_noangle(isnan(thrust_r_noangle))=0;
thrust_l_noangle=Fw.*sum_l;
thrust_l_noangle(isnan(thrust_l_noangle))=0;
thrust_b_noangle=Fw.*sum_b;
thrust_b_noangle(isnan(thrust_b_noangle))=0;
thrust_u_noangle=Fw.*sum_u;
thrust_u_noangle(isnan(thrust_u_noangle))=0;
% %-------------------------------------------------------------------------
% thrust_w(ff,:,:)=(sqrt(thrust_r.^2+thrust_l.^2+thrust_u.^2+thrust_b.^2)); % Thrust everywhere
thrust_w(ff,:,:)=((thrust_r+thrust_l+thrust_u+thrust_b)); % Thrust everywhere
% thrust_w_noangle(ff,:,:)=(sqrt(thrust_r_noangle.^2+thrust_l_noangle.^2+... % Thrust everywhere
without angle correction
% thrust_u_noangle.^2+thrust_b_noangle.^2));
thrust_w_noangle(ff,:,:)=((thrust_r_noangle+thrust_l_noangle+... % Thrust everywhere without angle
correction
thrust_u_noangle+thrust_b_noangle));
thrust_w_msl(ff,:,:)=bou_wd_msl_nan.*...
squeeze(thrust_w(ff,:,:)); % Thrust MEAN SEA LEVEL
thrust_w_wet(ff,:,:)=squeeze(bou_wd_nan(ff,:,:)).*... % Thrust along the WET CONTOUR
squeeze(thrust_w(ff,:,:));
thrust_w_noangle_msl(ff,:,:)=bou_wd_msl_nan.*... % Thrust MEAN SEA LEVEL without angle correction
squeeze(thrust_w_noangle(ff,:,:));
thrust_w_noangle_wet(ff,:,:)=squeeze(bou_wd_nan(ff,:,:)).*... % Thrust along the WET CONTOUR without
angle correction
squeeze(thrust_w_noangle(ff,:,:));
mask_wd_tonelli1=mask_wd;
%note:I INITIally used hc but then tought that it is better to use 0 in any case so you don't
%care about hc value used by user
% mask_wd_tonelli1(depth_all>hc & depth_all<0.2)=...
% %%%%---INITIAL WAVE THRUST REDUCTION %%%%
% mask_wd_tonelli1(depth_all>0 & depth_all<0.2)=...
% 1-0.45.*(depth_all(depth_all>0 & depth_all<0.2)./0.2); % Reduce up to 45% the thrust when 0.1< depth
<0.2
% mask_wd_tonelli1(depth_all>0.2 & depth_all<0.4)=...
% 0.55-0.55.*2.5.*(depth_all(depth_all>0.2 & depth_all<0.4)-0.2); % Reduce up to the 0.275% the thrust
when 0.2<depth<0.4
% mask_wd_tonelli1(depth_all>0.4)=0.275; % Constant reduction whent he depth is higher than 0.4
% mask_wd_tonelli(ff,:,:)=mask_wd_tonelli1; % Tonelli mask to use to reduce thrust when submerged
%
% thrust_w_tonelli(ff,:,:)=bou_wd_msl_nan.*... % Thrust along the WET CONTOUR without angle correction
% squeeze(thrust_w(ff,:,:)).*...
% mask_wd_tonelli1;
%
% thrust_w_tonelli(ff,:,:)=squeeze(bou_wd_nan(ff,:,:)).*... % Thrust along the WET CONTOUR without
angle correction
% squeeze(thrust_w(ff,:,:)).*...
% mask_wd_tonelli1;
%%%%%%---NEW REDUCTION %%%%
```

```
mask_wd_tonelli1(depth_all>0 & depth_all<0.4)=...
1-0.6.*(depth_all(depth_all>0 & depth_all<0.4)./0.4);
thrust_w_tonelli(ff,:,:)=bou_wd_msl_nan.*... % Thrust along the WET CONTOUR without angle correction
squeeze(thrust_w(ff,:,:)).*...
mask_wd_tonelli1;
thrust_w_tonelli(ff,:,:)=squeeze(bou_wd_nan(ff,:,:)).*... % Thrust along the WET CONTOUR without angle
correction
squeeze(thrust_w(ff,:,:)).*...
mask_wd_tonelli1;
% %---------------------------------------------------------------------
% % CALCULATE THE RISK PARAMETER
% %---------------------------------------------------------------------
% %---------------------------------------------------------------------
% % EROSION FACTOR AND WAVE FACTOR
% %---------------------------------------------------------------------
bstr=sqrt(bustr_rho.^2+bvstr_rho.^2).*cosd(exp_r-Dwave); % Shear stress asscoiated to each point
Area_cell=sqrt(l_x.*l_y); % Area associated to each rho point
% %-----------------------------------------------------------------------
% %CALCULATE THE WAVE POWER
% %-----------------------------------------------------------------------
wavenumber_k=2.*pi./(Lwave);
angular_frequency_sigma=sqrt(g.*wavenumber_k.*tanh(wavenumber_k.*depth));
group_celerity=0.5*(angular_frequency_sigma./wavenumber_k).*(1+(2.*wavenumber_k.*depth)./(sinh(2.*waven
umber_k.*depth)));
Pwave=group_celerity.*ro0.*9.81.*Hwave.^2./8;
Pwave2(ff,:,:)=Pwave;
Hwave2(ff,:,:)=Hwave;
l_r=(squeeze(bou_wd(ff,:,:)).*sum_r.*(l_y)); l_r(isnan(l_r)==1)=0;
l_l=squeeze(bou_wd(ff,:,:)).*sum_l.*(l_y); l_l(isnan(l_l)==1)=0;
l_u=squeeze(bou_wd(ff,:,:)).*sum_b.*(l_x); l_u(isnan(l_u)==1)=0;
l_b=squeeze(bou_wd(ff,:,:)).*sum_u.*(l_x); l_b(isnan(l_b)==1)=0;
ltot=l_r+l_l+l_u+l_b; % length of the areas which are NOT sheltered by other cells
EFstar(ff,:,:)=(Area_cell.*(abs(bstr)-bucr)); %******REMEMBER, YOU HAVE DONE THIS WITH TOTAL SHEAR
STRESS YOU CAN
SEPARATE CURRENT AND WAVE SHEAR STRESS( SEE OUTPUTS SWAN BUSTR_W BUSTR_C)
WFstar(ff,:,:)=((Pwave-Pcr).*ltot);
% %%%%%%%%%%%%%%%%%%%%%%%%
% if (n_T(gg+1)-(dt+dt.*ff))==0;
% % % If the time step is multiple of the time you want to average the Erosion/Wave factor
%
% % rem(dt_hour.*ff,T_hours)<=dt_hour;
%
% gg=gg+1;
% tf=squeeze(sum(bou_wd(ff-nn+1:ff,:,:),1)); % Sum the wet points at the boundary between different
times
% % Points different from zero are the wet boundary points for at leats
one time step
% tf(tf > percent)=1; % The defaul value fro percent is zero. meaning thet if one point is the
wet boundary for % at least one simulation time step It is part of the tidal flat
% tf(tf < percent)=0; % Don't consider tidal flat points below the percentage
% Atf(gg)=sum(sum(sum((l_x.*l_y).*tf))); % Tidal flat area is the sum of each cell area creating the
tidal flat.
%
% % EF(gg,:,:)=((squeeze(sum(EFstar(ff-nn:ff,:,:),1))./(T)));
% % WF(gg,:,:)=squeeze(sum(WFstar(ff-nn:ff,:,:),1))./(T);
%
% %i think I dont need to divide by T but by the number of layers that i
% %sum
% EF(gg,:,:)=((squeeze(sum(EFstar(ff-nn+1:ff,:,:),1))./(nn)));
% WF(gg,:,:)=squeeze(sum(WFstar(ff-nn+1:ff,:,:),1))./(nn);
% % % % % % % % % % % % % % % % % % % % % % % % % % % % % % % % % % % % % % % % % % % % %
%
% EF_tosum=EF(gg,:,:); % Create new variable for the erosion factor to delete NaN and set
them equal to zero
% EF_tosum(isnan(EF_tosum)==1)=0;
% WF_tosum=WF(gg,:,:);
% WF_tosum(isnan(WF_tosum)==1)=0; % Create new variable for the wave factor to delete NaN and set them
equal to zero
%
% EF_TOT(gg)=sum(EF_tosum(:))./Atf(gg);
% WF_TOT(gg)=sum(WF_tosum(:))./(sum(ltot(:)));
%
% end
% %%%%%%%%%%%%%%%%%%%%%%%%%%%%%%%%
end
hh=0;
```

```
for d=nn:nn:nt
hh=hh+1;
tf=squeeze(sum(bou_wd(d-nn+1:d,:,:),1)); % Sum the wet points at the boundary between different times
% Points different from zero are the wet boundary points for at leats
one time step
tf(tf > percent)=1; % The defaul value fro percent is zero. meaning thet if one point is the
wet boundary for % at least one simulation time step It is part of the tidal flat
tf(tf < percent)=0; % Don't consider tidal flat points below the percentage
Atf(hh)=sum(sum(sum((l_x.*l_y).*tf))); % Tidal flat area is the sum of each cell area creating the
tidal flat.
EF(hh,:,:)=((squeeze(sum(EFstar(d-nn+1:d,:,:),1))./(nn)));
WF(hh,:,:)=squeeze(sum(WFstar(d-nn+1:d,:,:),1))./(nn);
EF_tosum=EF(hh,:,:); % Create new variable for the erosion factor to delete NaN and set them
equal to zero
EF_tosum(isnan(EF_tosum)==1)=0;
WF_tosum=WF(hh,:,:);
WF_tosum(isnan(WF_tosum)==1)=0; % Create new variable for the wave factor to delete NaN and set them
equal to zero
EF_TOT(hh)=sum(EF_tosum(:))./Atf(hh);
WF_TOT(hh)=sum(WF_tosum(:))./(sum(ltot(:)));
end
```

```
------bin data-----
all1=(er);
all2=(thrust_mean_tonelli_all_new_isolated(dd30)');
latitude1=(coordinate(d_isolated(dd30),1));
longitude1=(coordinate(d_isolated(dd30),2));
all_12=[all1;all2;latitude1';longitude1']';
ap=find(latitude1<=39.54);
bp=find(longitude1<=-74.38);
as=find(latitude1>=39.7);
bs=find(longitude1>=-74.15);
cp=intersect(ap,bp);
cs=intersect(as,bs);
c=[1:length(all1)]';
for i=1:length(cs)
    ss(i)=find(c==cs(i));
end
c(ss)=[];
for i=1:length(cp)
    pp(i)=find(c==cp(i));
end
c(pp)=[];
all_12=[all1(c);all2(c);latitude1(c)';longitude1(c)']';
all12=sortrows(all_12,1);
latitude=all12(:,3);longitude=all12(:,4);
all12=all12(:,1:2);
% a=find(isnan(all12)==1)
% all12(a,:)=[];
maxi=nanmax(all12(:,1));
mini=nanmin(all12(:,1));
bins =linspace(mini, maxi, numbins);
% bins1=exp(linspace(log(0.00001),log(treshold),n));
% bins2 =linspace(treshold, maxi,numbins);
% bins=[bins1 bins2];
nn=length(all1)./(length(bins));
marker_index=[];
clear mu stdi mux stdi2 stdi1 marker_index
marker_index=[];
for k = 2:numbins-1
  ind = find(all12(:,1)<=bins(k) & all12(:,1)>bins(k-1));
  if (~isempty(ind))==1
    mu(k) = nanmean(all12(ind,1));
    stdi(k)=nanstd(all12(ind,1));
    mux(k)=nanmean(all12(ind,2));
    stdi2(k)=nanstd(all12(ind,2));
    lat(k)=nanmean(latitude(ind));
    latstd(k)=std(latitude(ind));
    long(k)=nanmean(longitude(ind));
    longstd(k)=std(longitude(ind));
  else
    mu(k) = nan;
    stdi(k)=nan;
    mux(k)=nan;
    stdi2(k)=nanstd(all12(ind,2));
  end
end
for k = 2:numbins-1
    if mux(k)>mux(k-1)
  ind = find(all12(:,2)<=mux(k) & all12(:,2)>=mux(k-1));
    elseif mux(k)<mux(k-1)
       ind = find(all12(:,2)<=mux(k-1) & all12(:,2)>=mux(k));
    end
  if (~isempty(ind));
    stdi1(k)=nanstd(all12(ind,1));
  else
     stdi1(k)=nan;
  end
end
mm=[mux;mu;stdi1;stdi2]';
mm(mm(:,1)==0,:)=[];
mm(mm(:,2)==0,:)=[];
```

```
mm(mm(:,2)<0.08)=nan;
figure
hold on
stem(mm(:,1),mm(:,2)+mm(:,3),'c','MarkerSize',2);
stem(mm(:,1),mm(:,2)-mm(:,3),'w','MarkerSize',1);
plot(mm(:,1),mm(:,2)-mm(:,3),'co','MarkerSize',2);
plot(mm(:,1),mm(:,2),'ro','MarkerFaceColor','r');
excel=[mm(:,1),mm(:,2)]
excel(isnan(mm(:,1))==1 | isnan(mm(:,2))==1,:)=[];
```

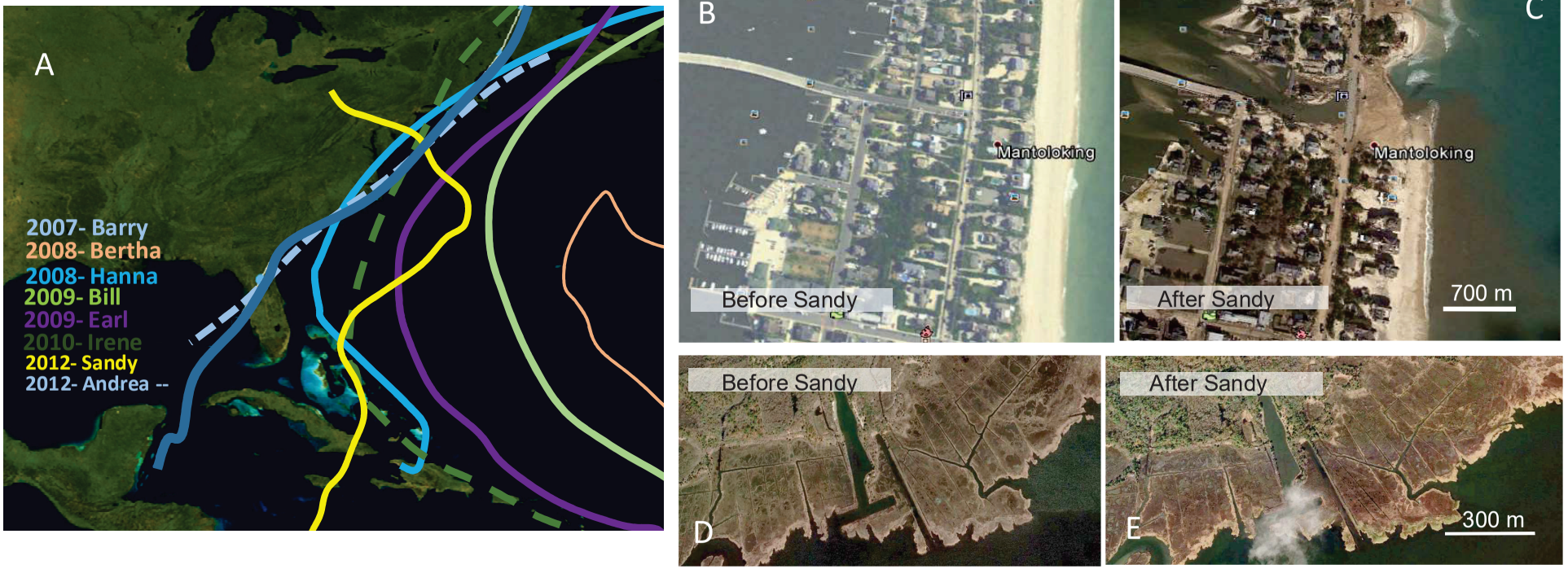
A
2007- Barry
2008- Bertha
2008- Hanna
2009- Bill
2009- Earl
2010- Irene
2012- Sandy
2012- Andrea --
B
Mantoloking
Before Sandy
C
Mantoloking
After Sandy
700 m
D
Before Sandy
E
After Sandy
300 m

Figure S1 A) Path of the major Hurricanes interesting New Jersey for the period from 2007 to 2013 (Data from National Hurricane Centre, http://www.nhc.noaa.gov/).

Of these, only Irene (2010), and Sandy (2012) made landfall in New Jersey ad caused Hurricane force winds in the area.

Sandy has been classified as the most destructive in the history of New Jersey [Blake et al., 2012; National Hurricane Center; Brandon et al., 2014].

B) Before and after Hurricane Sandy images for a sandy beach in Barnegat Bay (40° 2'25.99"N, 74° 2'55.38"W). Significant erosion is noticeable for this beach. Courtesy of Google Earth.

C) Before and after Hurricane Sandy images (40° 1'52.90"N, 74° 4'13.17"W) around 2 km distance from previous point. No significant erosion is noticeable for this salt marsh. Courtesy of Google Earth.

View publication stats